Applied Chemical Engineering (2025) Volume 8 Issue 1 ISSN: 2578-2010 (O)
doi: 10.59429/ace.v8i1.5652

ORIGINAL RESEARCH ARTICLE

Synthesis of Dioxane-fused Coumarins as a new class of biosafe multifunctional therapeutic candidates: A journey from *In Vitro* to *In Silico* prediction

Marwa Mohammed Alshaher, Yasser Fakri Mustafa*

Department of Pharmaceutical Chemistry, College of Pharmacy, University of Mosul, Mosul, 41001, Iraq

***Corresponding author:** Yasser Fakri Mustafa, Dr.yassermustafa@uomosul.edu.iq

ABSTRACT

This study presents for the first time the novel synthesis and in vitro-in silico bio-evaluation of seven coumarin derivatives linearly conjugated with a 1,4-dioxane ring. The primary goal was to develop accessible and modifiable coumarin-based scaffolds with a broad spectrum of biological activities. The structural identities of the synthesized compounds were confirmed using various spectroscopic techniques, including ^{1}H-NMR, ^{13}C-NMR, and FTIR analyses. The biological potential of the synthesized fused structures was systematically evaluated through a series of *in vitro* assays. Notably, **DFC4** emerged as a promising candidate with strong antioxidative stress activity. In terms of antidiabetic potential, **DFC2** demonstrated significant inhibition of both α-glucosidase and α-amylase enzymes, suggesting its usefulness in managing hyperglycemia. **DFC5** exhibited potent antibacterial effects, comparable to those of ciprofloxacin, against all tested aerobic bacterial strains. In addition, **DFC1** showed superior antifungal activity, outperforming nystatin. The same fused structure also displayed noteworthy anti-inflammatory properties, likely through a cyclooxygenase-dependent mechanism. Regarding anticancer properties, **DFC4** again stood out by exhibiting effective cytotoxicity toward cancer cells while maintaining biosafety toward non-carcinogenic cells. All synthesized fused structures, especially **DFC5**, demonstrated favorable biosafety profiles when tested against commensal bacterial strains. To complement the *in vitro* findings, computational tools were used to predict the toxicity and pharmacokinetic profiles of the structures under evaluation. The results indicated that the synthesized fused structures possess desirable biosafety thresholds and oral bioavailability characteristics. Collectively, these findings suggest that the newly synthesized fused structures hold significant potential as multifunctional therapeutic agents for future drug development.

Keywords: coumarin; 1,4-dioxane; conjugation; biosafety; multifunctional therapeutics

ARTICLE INFO

Received: 1 April 2025
Accepted: 27 April 2025
Available online: 30 April 2025

1. Introduction

Heterocyclic compounds are a class of cyclic organic molecules that include at least one atom other than carbon, commonly nitrogen, oxygen, or sulfur, within their ring structure. However, heterocycles containing other types of heteroatoms are also well documented[1]. Due to their diverse biological activities, heterocyclic compounds play a crucial role in various fields of life sciences and are considered essential in medicinal chemistry[2]. Many biologically significant molecules, such as hemoglobin, vitamins, DNA, and RNA, are based on heterocyclic frameworks. Their wide structural diversity and functional versatility make them valuable scaffolds in the development of pharmaceutical drugs for treating a broad range of diseases[3].

Coumarin, or α-benzopyrone, which comprises fused benzene and α-pyrone rings[4], is a prominent member of the heterocyclic family,

recognized for its extensive and varied biological activities. These include antioxidant[5–7], antidiabetic[8–10], antibacterial[11–13], antifungal[14–16], anti-inflammatory[17–19], anticancer[20–22], antitubercular[23–25], antiviral[26–28], antidepressant[29–31] and anticoagulant[32–34] properties. Coumarin molecules can be derived naturally from plants[35–37] or manufactured chemically in laboratories[38–40]. Besides these, different bacteria and fungi have also been found to make many coumarins[41–43].

Substitution may occur at any of the six available positions, and the variety of substitutions and fusions offers a broad array of possible configurations, which may elucidate the common occurrence of coumarin-based derivatives in nature[44,45]. The coumarin scaffold is present in various physiologically active compounds that play a crucial role in medicine and therapies[46,47]. They are primarily utilized in the pharmaceutical sector, and due to their exceptional luminous properties, they serve as detectors for various biological components[48,49], ion sensors[50], and applications in the laser business[51]. Additionally, due to their pleasant fragrance, they are utilized as distinctive ingredients in fragrances and cosmetics[52]. coumarins have numerous appealing characteristics that facilitate their application in various fields, including their uncomplicated structure with low molecular weight, straightforward production and modification, minimal toxicity, favorable bioavailability, and widespread occurrence in nature[53–55]. Compounds containing coumarin attract global scientific interest to investigate their bioactive potential both *in vitro* and *in vivo*, with considerable confidence in identifying promising treatment options for various disorders[56–58].

1,4-Dioxane (DO) is a colorless, flammable liquid characterized by a subtle, sweet fragrance, commonly acknowledged for its function as a solvent in industrial and scientific settings. It is a six-membered cyclic ether with two oxygen atoms that enhance its chemical stability and extensive solvent compatibility[59]. This distinctive configuration enables it to blend effortlessly with both polar and non-polar molecules, rendering it particularly advantageous for dissolving compounds with low solubility and fostering consistent conditions in chemical reactions. Consequently, DO functions as an efficient reaction medium in organic synthesis, especially in catalytic and polymerization processes, and is frequently employed to stabilize chlorinated solvents[60,61].

From an electrical perspective, DO exhibits considerable electron-donating properties, principally due to the lone electron pairs on its oxygen atoms. Despite being less nucleophilic than conventional amines, its oxygen atoms can participate in dipole–dipole interactions and function as hydrogen bond acceptors, especially with donor groups such as N–H and O–H[62]. This renders it an efficient stabilizer of positively charged intermediates and transition states, particularly in reactions involving electron-deficient heterocyclic systems like pyridinium ions or nitro-substituted aromatic compounds. Notably, the linear introduction of DO at the 6,7-position of coumarin scaffolds can improve the overall physicochemical features of the resultant molecules. This alteration has demonstrated enhanced binding interactions with biological targets, such as enzymes and receptors, resulting in augmented pharmacological activity[63]. Consequently, DO serves as both a valuable solvent and a significant structural element in the formulation of bioactive molecules in pharmaceutical and heterocyclic chemistry[64,65].

The process of combining two or more different cyclic chemicals to create synthesized fused structures with beneficial biological activities is known as ring conjugation. The frameworks that are produced have the ability to simultaneously target and utilize two distinct enzymes and/or receptors, resulting in strong and beneficial synergistic interactions[66–68]. As a result, a single conjugated entity can overcome drug resistance obstacles and provide numerous unique modes of action, which is advantageous in cancer chemotherapy as well as others. Additionally, this approach may improve medication metabolism, absorption, and other pharmacokinetic aspects[69–71].

Medicinal chemists have been fascinated by the investigation of the synthesis of various heterocyclic coumarin conjugates. By carefully combining the coumarin rings with different heterocycles, such as

pyrrole[72], furan[73], pyran[74], oxepine[75], and oxazole[76], these conjugates are created. The heterocyclic moiety is incorporated as a substituent through sigma bond connectors at various locations throughout the coumarin framework or as an essential component of a benzene and/or α-pyrone ring to accomplish such conjugation. This creative conjugation of molecular entities has produced substances with remarkable biological activities that have a great deal of promise for use in medicine as shown in the previous work of Jasim and Mustafa[77–79], Waheed and Mustafa[80–82], Jibroo and Mustafa[83], as well as Zeki and Mustafa[57,84–88].

This study aims to explore the biological activities of seven novel dioxane-fused coumarins (DFCs), each incorporating a DO ring conjugated linearly at the 6,7-position of the benzene ring within the coumarin framework. These compounds, designated as **P-DFC** and **DFC1**-**DFC7**, were first evaluated for their antioxidant activity by assessing their ability to neutralize reactive oxygen species. Additionally, their antidiabetic potential was examined by measuring their inhibitory effects on two key metabolic enzymes, porcine α-amylase and yeast α-glucosidase. To determine their antibacterial properties, the DFCs were tested *in vitro* using the broth dilution method against six aerobic gram-negative (AG^{-ve}) bacterial strains, including Pseudomonas aeruginosa, Klebsiella pneumoniae, Haemophilus influenzae, Escherichia coli, Salmonella typhi, and Shigella dysenteriae, as well as four anaerobic (ANA) bacterial strains: Bacteroides fragilis, Clostridium perfringens, Fusobacterium necrophorum, and Prevotella melaninogenica. Their antifungal efficacy was also evaluated against two fungal strains, *Candida albicans* and *Aspergillus niger*. Additionally, the anti-inflammatory potential of DFCs was determined by examining their ability to inhibit cyclooxygenase (COX) enzymes (COX-1 and COX-2). Furthermore. The anticancer potential of the structures under study was investigated through the MTT assay against six cancer cell lines: AMN-3, HeLa, KYSE-30, MCF-7, SKG, and SK-OV-3. Finally, the biosafety of the derivatives was assessed by testing their effects on three non-pathogenic bacterial strains: *Escherichia coli* (BAA-1427), *Escherichia coli* (MG-1655), and *Escherichia coli* (BAA-1430). To further evaluate their safety, the biocompatibility with normal human cell lines was checked (HEK-293, MCF-10A, and RWPE-1). The *in-silico* study was simple and straightforward, and it was performed to evaluate the possible harm and pharmacokinetic profiles of the synthesized DFCs using computational tools including ProTox-II, SwissADME, and PreADMET. This assessment focused on essential safety measures, including cytotoxicity, carcinogenic potential, and hepatotoxicity, alongside drug-likeness characteristics such as gastrointestinal absorption, metabolic stability, and oral bioavailability. The insights derived from these predictive models enabled the identification of the most promising drugs with advantageous safety and pharmacokinetic properties for further development.

2. Experimental section

2.1. Equipments, chemicals, and bioreagents

Several foreign sources provided the chemicals and bioreagents required to complete the synthesis process and assess the synthesized fused structures' potential for use in medicine. Key Organics Ltd., Bio-Vision, Haihang, Chambrau, Bioworld, BT-LAB, Labcorp, and Sigma-Aldrich were some of these vendors. The melting point (m.p.) values of **P-DFC** and **DFC1**-**DFC7** were determined using the CIA 9300 automated instrument. The quality of the DFCs was verified, and the reaction's progress was tracked using thin-layer chromatography (TLC). The analytical approach applied in this investigation used silica gel as the stationary phase and a mobile phase made up of acetone and chloroform in a 4:1 ratio. The Bruker ATR (of the Alpha model), the Avance III HD machine (made by Bruker and used DMSO-*d*6 as a solvent), which runs at 75 MHz for ^{13}C and 300 MHz for ^{1}H, and the UV-1600PC UV–Vis spectrophotometer was used to analyze the infrared (IR), nuclear magnetic resonance (NMR), and ultraviolet-visible (UV-Vis) spectra of the synthesized compounds, respectively. **Figure 1** delineated the synthetic procedures requisite for the synthesis of the target coumarins.

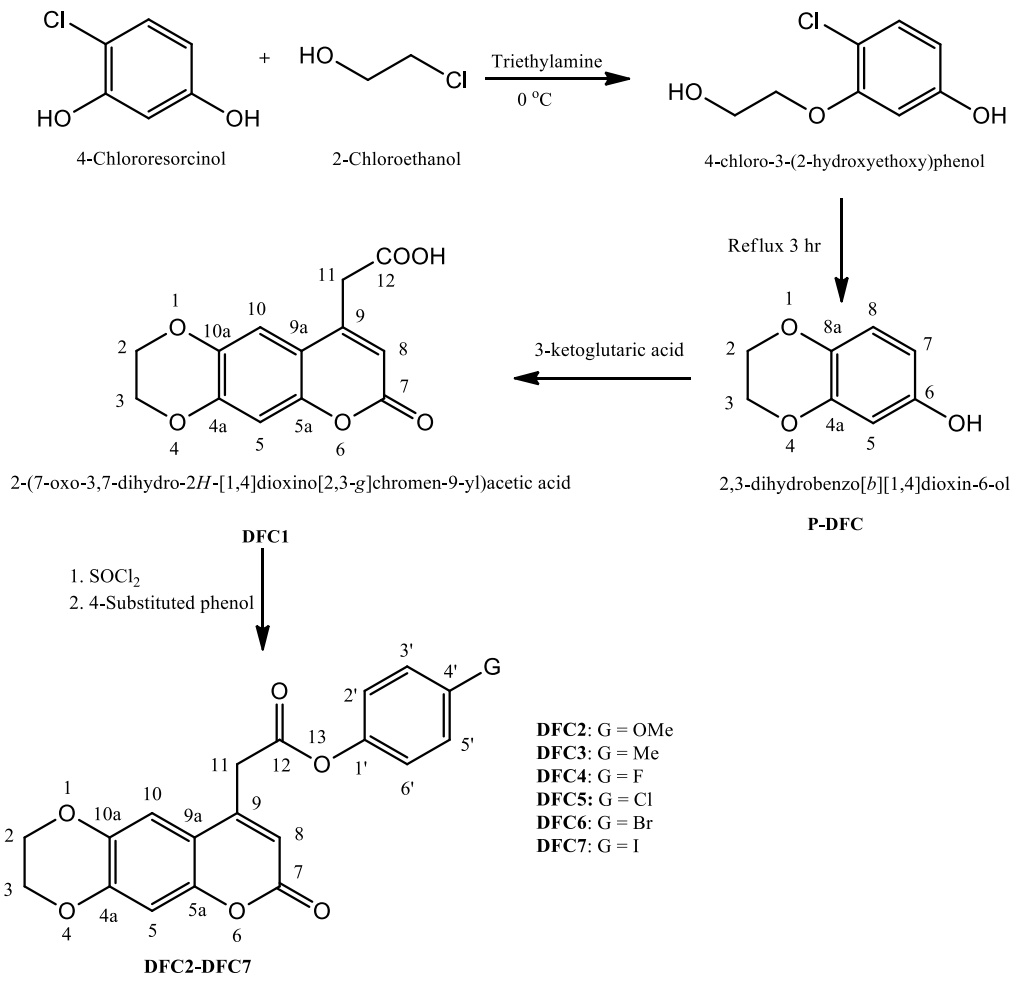

Figure 1. The synthetic pathway of P-DFC and DFC1-DFC7.

2.2. Synthesis of P-DFC

A 40-ml mixture of dried ethyl acetate with Na2SO4, 1.45 g of 4-chlororesorcinol (10 mmol), and 0.5 ml of triethylamine was made. This mixture was then put in a salt-ice bath to help the reaction happen. The reagent named 2-chloroethanol (0.67 ml, 10 mmol) was pipetted into this solution at a frequency of one drop per minute. The working mixture was stirred for 2 hours and refluxed for 3 hours. 50 ml of distilled water was added to the crude solution, and the organic layer was separated and evaporated. This left behind **P-DFC**, which is a brown oil that is yielded at 76.24%, has a boiling point of 294-296°C, and has a density of 1.32 g/ml[89].

P-DFC: Brown oil; λmax (ethanol) = 442 nm; Percentage of yield (weight acquired at lab setting) = 76.24 (0.58 ml, 0.77 g); Rf (chloroform and acetone mixed at the ration of 4-to-1) = 0.21; B.p. = 294-296°C; IR *v*max: 3304 cm^{-1} (broad-stretching band, H-bonding phenol O-H functional moiety), 1598 cm^{-1} (medium-stretching band, arene C=C functional moiety), and 1260 as well as 1055 cm^{-1} (strong-stretching band, cyclic ether C-O-C functional moiety); ^{1}H-NMR (DMSO-*d*6 , 300 MHZ): δ = 7.08 ppm (doublet peak, *J* = 6 Hz, 1H, proton-8), δ = 6.82 ppm (doublet peak, 1H, *J* = 6 Hz, proton-7), δ = 6.56 ppm (singlet peak, 1H, proton-5), δ = 5.50 ppm (singlet peak, 1H, proton at position HO-6), and δ = 4.26 ppm (singlet peak, 4H, protons at position 2 and 3); ^{13}C-NMR (DMSO-*d*6, 75 MHz): δ = 157.8 ppm (C, 6-carbon), δ = 151.5 ppm (C, 4a-carbon), δ = 149.2 ppm (C, 8a-carbon), δ = 125.3 ppm (CH, 8-carbon), δ = 120.0 ppm (CH, 7-carbon), δ = 110.1 ppm (CH, 5-carbon), and δ = 72.52 ppm (CH2, carbons at position 2 and 3).

2.3. Synthesis of DFC1

A mixture of 0.58 ml of **P-DFC** (5 mmol) and 0.88 g of 3-ketoglutaric acid (6 mmol) was gently heated to produce a clear solution of ethyl acetate. The mixture was incrementally introduced into a round-bottom flask holding 25 ml of concentrated H_2SO_4 while sustaining a temperature below 10°C with a salted ice bath. Following continuous stirring for 2.5 hours, the running liquid was removed from the ice bath and allowed to remain at room temperature on the stir plate overnight. The next day, we heated the mixture to 80°C to eliminate the original solvent, moved it to a beaker, and combined it with water and crushed ice. The precipitate was gathered with filter paper, washed with cold water, and air-dried at ambient temperature to produce **DFC-1**. The purification procedure utilized recrystallization from an ether-ethanol combination[90].

DFC1: Pale yellowish powder; λmax (ethanol) = 363 nm; Percentage of yield (weight acquired at lab setting) = 80.15 (1.05 g); Rf (chloroform and acetone mixed at the ration of 4-to-1) = 0.14; m.p. = 129-132°C; Solvent for recrystallization = mixture of diethylether and ethanol in an equal portion; IR *v*max: 3062 cm^{-1} (weak-stretching band, *cis* c=c functional moiety of the pyrone ring), 3015 cm^{-1} (centered-broad-stretching band, carboxylic acid-OH functional moiety), 2892 cm^{-1} (weak-stretching band, alkane C-H functional moiety), 1731 cm^{-1} (strong-stretching band, C=O functional moiety of the pyrone ring), 1689 cm^{-1} (strong-stretching band, aliphatic carboxylic acid C=O functional moiety), 1587 cm^{-1} (medium-stretching band, arene C=C functional moiety), and 1267 as well as 1066 cm^{-1} (strong-stretching bands, dioxane ether C-O-C functional moiety); ^{1}H-NMR (DMSO-*d*6 , 300 MHZ): δ = 11.13 ppm (singlet peak, 1H, carboxylic acid proton), δ = 7.96 ppm (singlet peak, 1H, proton-10), δ = 7.11 ppm (singlet peak, 1H, proton-5), δ = 6.39 ppm (singlet peak, 1H, proton-8), δ = 4.27 ppm (singlet peak, 4H, protons at positions 2 and 3) and 3.13 ppm (singlet peak, 2H, protons at position 11); ^{13}C-NMR (DMSO-*d*6, 75 MHz): δ = 173.7 ppm (C, 12-carbon), δ = 162.5 ppm (C, 7-carbon), δ = 154.0 ppm (C, 9-carbon), δ = 153.6 ppm (CH, 4a-carbon), δ = 152.4 ppm (C, 10a-carbon), δ = 151.5 ppm (C, 5a-carbon), δ = 127.5 ppm (C, 9a-carbon), δ = 125.2 ppm (CH, 10-carbon), δ = 115.7 ppm (CH, 5-carbon), 113.5 ppm (CH- 8-carbon), δ = 72.6 ppm (CH_2, carbons at positions 2 and 3), and δ = 31.0 ppm (CH_2, 11-carbon).

2.4. General method for the synthesis of DFC2-DFC7

A round-bottomed flask with two necks that held 1.31 g (5 mmol) of **DFC1** dissolved in 25 ml of freshly distilled $SOCl_2$ was put in a salt-ice bath. One of the necks was equipped with a condenser, while the other was sealed with a blue litmus paper stopper. The mixture was intentionally agitated for 30 minutes under anhydrous circumstances, thereafter, permitted to settle at room temperature for an additional 30 minutes, and finally refluxed for three hours. The color shift of the litmus paper, occurring every 30 minutes, facilitated the monitoring of the reaction's development. Once the color change in the blue litmus paper ceased, the excess of $SOCl_2$ was distilled off under reduced pressure. The white stuff that was left in the flask showed that the acyl chloride derivative of **DFC1** had been made[91]. A 40 ml solution of dehydrated diethyl ether was put into the same flask that still had the white precipitate in it. This solution comprises 5 mmol of 4-methoxyphenol and 1 ml of pyridine. The addition was performed at ambient temperature, and the mixture was refluxed after being agitated under anhydrous conditions for 30 minutes. As mentioned earlier, the change in the color of the litmus paper was utilized to monitor the reaction's progress. Upon completion of the reaction, 50 ml of water was incorporated into the mixture. **DFC2** was subsequently produced by isolating, desiccating, and evaporating the organic layer[92]. The identical technique was applied with many 4-substituted phenols, specifically 4-methylphenol, 4-fluorophenol, 4-chlorophenol, 4-bromophenol, and 4-iodophenol, yielding **DFC3**, **DFC4**, **DFC5**, **DFC6**, and **DFC7**, respectively. The recrystallization procedure utilized mixes of ether and ethyl acetate in ratios of 1:3 (for **DFC2** and **DFC3**) and 1:2 for the remaining DFCs[93].

DFC2: Slightly yellowish powder; λmax (ethanol) = 397 nm; Percentage of yield (weight acquired at lab setting) = 86.12 (1.52 g); Rf (chloroform and acetone mixed at the ration of 4-to-1) = 0.55; m.p. = 109-111°C; Solvent for recrystallization = mixture of diethyl ether and ethyl acetate in the ration of (1:3); IR *v*max: 3094 cm^{-1} (medium-stretching band, *cis* =C-H functional moiety), 2919 cm^{-1} (medium-stretching band, methoxy C-H functional moiety), 2822 cm^{-1} (weak-stretching band, alkane C-H functional moiety), 1733 cm^{-1} (strong-stretching band, C=O functional moiety of the pyrone ring), 1710 cm^{-1} (strong-stretching band, aliphatic ester C=O functional moiety), 1666 cm^{-1} (strong-stretching band, *cis* C=C functional moiety), 1594 cm^{-1} (strong-stretching band, arene C=C functional moiety), and 1266 as well as 1030 cm^{-1} (strong-stretching band, cyclic ether C-O-C functional moiety); ^{1}H-NMR (DMSO-*d*6 , 300 MHZ): δ = 7.95 ppm (singlet peak, 1H, proton-10), δ = 7.12 ppm (singlet peak, 1H, proton-5), δ = 7.04 ppm (doublet peak, *J* = 6 HZ, 2H, protons at positions 3'and 5'), δ = 6.78 ppm (doublet peak, *J* = 6 HZ, 2H, protons at positions 2' and 6'), δ = 6.35 ppm (singlet peak, 1H, proton-8), δ = 4.26 ppm (singlet peak, 4H, protons at positions 2 and 3), δ = 4.00 ppm (singlet peak, 3H, proton at position 4'-OCH3), and δ = 3.10 ppm (singlet peak, 2H, proton-11); ^{13}C-NMR (DMSO-*d*6, 75 MHz): δ = 169.6 ppm (C, 12-carbon), δ = 162.4 ppm (C, 7-carbon), δ = 156.4 ppm (C, 4'-carbon), δ = 154.7 ppm (C, 4a-carbon), δ = 153.0 ppm (C, 9-carbon), δ = 152.4 ppm (C, 10a-carbon), δ = 151.8 ppm (C, 5a-carbon), δ = 144.7 ppm (C, 1'-carbon), δ = 127.4 ppm (C, 9a-carbon), 120.3 ppm (CH, carbons at positions 3' and 5'), δ = 119.3 ppm (CH, 10-carbon), δ = 115.9 ppm (CH, 8-carbon), δ = 113.4 ppm (CH, 5-carbon), δ = 112.4 ppm (CH, carbons at positions 2' and 6'), δ = 72.5 ppm (CH_2, carbons at positions 2 and 3), δ = 51.0 ppm (CH_3, carbon at position 4'-OCH3), and δ = 28.2 ppm (CH_2, 11-carbon).

DFC3: Slightly yellowish powder; λmax (ethanol) = 390 nm; Percentage of yield (weight acquired at lab setting) = 85.09 (1.44 g); Rf (chloroform and acetone mixed at the ration of 4-to-1) = 0.53; m.p. = 106-108°C; Solvent for recrystallization = mixture of diethyl ether and ethyl acetate in the ration of (1:3); IR v_{max} (**Figure S10**): 3091 cm^{-1} (medium-stretching band, *cis* =C-H functional moiety), 2820 cm^{-1} (weak-stretching band, alkane C-H functional moiety), 1733 cm^{-1} (strong-stretching band, C=O functional moiety of the pyrone ring), 1713 cm^{-1} (strong-stretching band, aliphatic ester C=O functional moiety), 1666 cm^{-1} (strong-stretching band, *cis* C=C functional moiety), 1594 cm^{-1} (strong-stretching band, arene C=C functional moiety), and 1264 as well as 1026 cm^{-1} (strong-stretching band, cyclic ether C-O-C functional moiety); ^{1}H-NMR (DMSO-*d*6 , 300 MHZ) (**Figure S11**): δ = 7.92 ppm (singlet peak, 1H, proton-10), δ = 7.23 ppm (doublet peak, *J* = 6 HZ, 2H, protons at positions 3' and 5'), δ = 7.09 ppm (singlet peak, 1H, proton-5), δ = 7.03 ppm (doublet peak, *J* = 6 HZ, 1H, protons at positions 2' and 6'), δ = 6.36 ppm (singlet peak, 1H, proton-8), δ = 4.25 ppm (singlet peak, 4H, protons at positions 2 and 3), δ = 3.12 ppm (singlet peak, 2H, proton-11), and δ = 2.75 ppm (singlet peak, 3H, proton at position 4'-CH3); ^{13}C-NMR (DMSO-*d*6, 75 MHz) (**Figure S12**): δ = 169.1 ppm (C, 12-carbon), δ = 162.8 ppm (C, 7-carbon), δ = 154.3 ppm (C, 4a-carbon), δ = 153.0 ppm (C, 9-carbon), δ = 152.5 ppm (C, 10a-carbon), δ = 151.8 ppm (C, 5a-carbon), δ = 149.3 ppm (C, 1'-carbon), δ = 134.7 ppm (C, 4'-carbon), δ = 127.5 ppm (C, 9a-carbon), 125.8 ppm (CH, 10-carbon), δ = 122.6 ppm (CH, carbons at positions 3' and 5'), δ = 119.3 ppm (CH, carbons at positions 2' and 6'), δ = 115.7 ppm (CH, 8-carbon), δ = 114.0 ppm (CH, 5-carbon), δ = 72.6 ppm (CH_2, carbons at positions 2 and 3), δ = 27.5 ppm (CH_2, 11-carbon), and δ = 24.4 ppm (CH_3, carbon at position 4'-CH3).

DFC4: Off-white powder; λmax (ethanol) = 331 nm; Percentage of yield (weight acquired at lab setting) = 47.81 (0.82 g); Rf (chloroform and acetone mixed at the ration of 4-to-1) = 0.36; m.p. = 116-119°C; Solvent for recrystallization = mixture of diethyl ether and ethyl acetate in the ration of (1:2); IR *v*max: 3070 cm^{-1} (medium-stretching band, *cis* =C-H functional moiety), 2821 cm^{-1} (weak-stretching band, alkane -C-H functional moiety), 1733 cm^{-1} (strong-stretching band, C=O functional moiety of the pyrone ring), 1711 cm^{-1} (strong-stretching band, aliphatic ester C=O functional moiety), 1668 cm^{-1} (strong-stretching band, *cis* C=C functional moiety), 1593 cm^{-1} (strong-stretching band, arene C=C functional moiety), 1214 as well as 1026 cm^{-1} (strong-stretching band, cyclic ether C-O-C functional moiety), and 1075 cm^{-1} (strong-stretching band,

arene C-F functional moiety); ^{1}H-NMR (DMSO-*d*6 , 300 MHZ): δ = 7.91 ppm (singlet peak, 1H, proton-10), δ = 7.25 ppm (doublet peak, *J* = 6 HZ, 2H, protons at positions 2' and 6'), δ = 7.07 ppm (singlet peak, 1H, proton-5), δ = 7.02 ppm (doublet peak, *J* = 6 HZ, 2H, protons at positions 3' and 5'), δ = 6.34 ppm (singlet peak, 1H, proton-8), δ = 4.24 ppm (singlet peak, 4H, protons at positions 2 and 3), and δ = 3.12 ppm (singlet peak, 2H, proton-11); ^{13}C-NMR (DMSO-*d*6, 75 MHz): δ = 169.5 ppm (C, 12-carbon), δ = 161.1 ppm (C, 7-carbon), δ = 158.5 ppm (C, 4'-carbon), δ = 154.2 ppm (C, 4a-carbon), δ = 153.0 ppm (C, 9-carbon), δ = 152.6 ppm (C, 10a-carbon), δ = 151.8 ppm (C, 5a-carbon), δ = 147.9 ppm (C, 1'-carbon), δ = 127.5 ppm (C, 9a-carbon), 120.7 ppm (CH, carbons at positions 2' and 6'), δ = 119.6 ppm (CH, 10-carbon), δ = 115.8 ppm (CH, 8-carbon), δ = 113.4 ppm (CH, 5-carbon), δ = 108.4 ppm (CH, carbons at positions 3' and 5'), δ = 72.5 ppm (CH_2, carbons at positions 2 and 3), and δ = 27.5 ppm (CH_2, 11-carbon).

DFC5: Off-white powder; λmax (ethanol) = 336 nm; Percentage of yield (weight acquired at lab setting) = 54.28 (0.97 g); Rf (chloroform and acetone mixed at the ration of 4-to-1) = 0.36; m.p. = 120-123°C; Solvent for recrystallization = mixture of diethyl ether and ethyl acetate in the ration of (1:2); IR *v*max: 3070 cm^{-1} (medium-stretching band, *cis* =C-H functional moiety), 2823 cm^{-1} (weak-stretching band, alkane -C-H functional moiety), 1733 cm^{-1} (strong-stretching band, C=O functional moiety of the pyrone ring), 1713 cm^{-1} (strong-stretching band, aliphatic ester C=O functional moiety), 1667 cm^{-1} (strong-stretching band, *cis* C=C functional moiety), 1594 cm^{-1} (strong-stretching band, arene C=C functional moiety), 1262 as well as 1066 cm^{-1} (strong-stretching band, cyclic ether C-O-C functional moiety), and 986 cm^{-1} (strong-stretching band, arene C-Cl functional moiety); ^{1}H-NMR (DMSO-*d*6 , 300 MHZ): δ = 7.90 ppm (singlet peak, 1H, proton-10), δ = 7.51 ppm (doublet peak, *J* = 6 HZ, 2H, protons at positions 3' and 5'), δ = 7.33 ppm (doublet peak, *J* = 6 HZ, 2H, protons at positions 2' and 6'), δ = 7.08 ppm (singlet peak, 1H, proton-5), δ = 6.35 ppm (singlet peak, 1H, proton-8), δ = 4.25 ppm (singlet peak, 4H, protons at positions 2 and 3), and δ = 3.14 ppm (singlet peak, 2H, proton-11); ^{13}C-NMR (DMSO-*d*6, 75 MHz): δ = 169.3 ppm (C, 12-carbon), δ = 162.2 ppm (C, 7-carbon), δ = 154.4 ppm (C, 4a-carbon), δ = 153.0 ppm (C, 9-carbon), δ = 152.5 ppm (C, 10a-carbon), δ = 151.7 ppm (C, 5a-carbon), δ = 150.4 ppm (C, 1'-carbon), δ = 132.0 ppm (C, 4'-carbon), δ = 127.5 ppm (C, 9a-carbon), 125.1 ppm (CH, 10-carbon), δ = 122.9 ppm (CH, carbons at positions 3' and 5'), δ = 120.5 ppm (CH, carbons at positions 2' and 6'), δ = 115.8 ppm (CH, 8-carbon), δ = 113.4 ppm (CH, 5-carbon), δ = 72.6 ppm (CH_2, carbons at positions 2 and 3), and δ = 33.2 ppm (CH_2, 11-carbon).

DFC6: Gray-white powder; λmax (ethanol) = 306 nm; Percentage of yield (weight acquired at lab setting) = 40.98 (0.83 g); Rf (chloroform and acetone mixed at the ration of 4-to-1) = 0.42; m.p. = 116-118°C; Solvent for recrystallization = mixture of diethyl ether and ethyl acetate in the ration of (1:2); IR *v*max: 3069 cm^{-1} (medium-stretching band, *cis* =C-H functional moiety), 2820 cm^{-1} (weak-stretching band, alkane -C-H functional moiety), 1731 cm^{-1} (strong-stretching band, C=O functional moiety of the pyrone ring), 1709 cm^{-1} (strong-stretching band, aliphatic ester C=O functional moiety), 1666 cm^{-1} (strong-stretching band, *cis* C=C functional moiety), 1595 cm^{-1} (strong-stretching band, arene C=C functional moiety), 1267 as well as 1065 cm^{-1} (strong-stretching band, cyclic ether C-O-C functional moiety), and 900 cm^{-1} (strong-stretching band, arene C-Br functional moiety); ^{1}H-NMR (DMSO-*d*6 , 300 MHZ): δ = 7.95 ppm (singlet peak, 1H, proton-10), δ = 7.73 ppm (doublet peak, *J* = 6 HZ, 2H, protons at positions 3' and 5'), δ = 7.14 ppm (singlet peak, 1H, proton-5), δ = 6.94 ppm (doublet peak, *J* = 6 HZ, 2H, protons at positions 2' and 6'), δ = 6.37 ppm (singlet peak, 1H, proton-8), δ = 4.23 ppm (singlet peak, 4H, protons at positions 2 and 3), and δ = 3.13 ppm (singlet peak, 2H, proton-11); ^{13}C-NMR (DMSO-*d*6, 75 MHz): δ = 169.2 ppm (C, 12-carbon), δ = 162.2 ppm (C, 7-carbon), δ = 154.4 ppm (C, 4a-carbon), δ = 153.1 ppm (C, 9-carbon), δ = 152.5 ppm (C, 10a-carbon), δ = 151.8 ppm (C, 5a-carbon), δ = 151.3 ppm (C, 1'-carbon), δ = 127.5 ppm (C, 9a-carbon), δ = 125.2 ppm (C, 10-carbon), 123.6 ppm (CH, carbons at positions 3' and 5'), δ = 121.3 ppm (CH, carbons at positions 2' and 6'), δ = 118.5 ppm (C, 4'-carbon), δ = 115.8 ppm (CH, 8-carbon), δ = 113.4 ppm (CH, 5-carbon), δ = 72.6 ppm (CH_2, carbons at positions 2 and 3), and δ = 33.2 ppm (CH_2, 11-carbon).

DFC7: Gray-white powder; λmax (ethanol) = 311 nm; Percentage of yield (weight acquired at lab setting) = 41.87 (0.94 g); Rf (chloroform and acetone mixed at the ration of 4-to-1) = 0.44; m.p. = 123-125°C; Solvent for recrystallization = mixture of diethyl ether and ethyl acetate in the ration of (1:2); IR *v*max: 3067 cm^{-1} (medium-stretching band, *cis* =C-H functional moiety), 2826 cm^{-1} (weak-stretching band, alkane -C-H functional moiety), 1733 cm^{-1} (strong-stretching band, C=O functional moiety of the pyrone ring), 1711 cm^{-1} (strong-stretching band, aliphatic ester C=O functional moiety), 1664 cm^{-1} (strong-stretching band, *cis* C=C functional moiety), 1590 cm^{-1} (strong-stretching band, arene C=C functional moiety), 1268 as well as 1063 cm^{-1} (strong-stretching band, cyclic ether C-O-C functional moiety), and 864 cm^{-1} (strong-stretching band, arene C-I functional moiety); ^{1}H-NMR (DMSO-*d*6 , 300 MHZ): δ = 7.92 ppm (singlet peak, 1H, proton-10), δ = 7.85 ppm (doublet peak, *J* = 6 HZ, 2H, protons at positions 3' and 5'), δ = 7.12 ppm (singlet peak, 1H, proton-5), δ = 6.83 ppm (doublet peak, *J* = 6 HZ, 2H, protons at positions 2' and 6'), δ = 6.34 ppm (singlet peak, 1H, proton-8), δ = 4.24 ppm (singlet peak, 4H, protons at positions 2 and 3), and δ = 3.13 ppm (singlet peak, 2H, proton-11); ^{13}C-NMR (DMSO-*d*6, 75 MHz): δ = 169.5 ppm (C, 12-carbon), δ = 162.2 ppm (C, 7-carbon), δ = 154.5 ppm (C, 4a-carbon), δ = 153.1 ppm (C, 9-carbon), δ = 152.6 ppm (C, 10a-carbon), δ = 151.8 ppm (C, 5a-carbon), δ = 151.2 ppm (C, 1'-carbon), δ = 129.6 ppm (CH, carbons at positions 3' and 5'), δ = 127.7 ppm (C, 9a-carbon), 125.1 ppm (CH, 10-carbon), δ = 120.7 ppm (CH, carbons at positions 2' and 6'), δ = 115.8 ppm (CH, 8-carbon), δ = 113.4 ppm (CH, 5-carbon), δ = 93.0 ppm (C, 4'-carbon), δ = 72.6 ppm (CH_2, carbons at positions 2 and 3), and δ = 33.2 ppm (CH_2, 11-carbon).

3. Evaluation of the biological activities

3.1. Antioxidative stress evaluation

With an initial cell population of 12 × 10^3, the SH-SY5Y human neuroblastoma cell line (ATCC:CRL-2266) was employed in the current evaluation. The cells under study were moved from a growth plate with DMEM/F-12 medium (brochure number 11320033) to a dark, flat-bottomed surface plate with 96 wells. Following culture, the cells were exposed to an oxidative stressor for 24 hours, specifically 100 μM H_2O_2. Following exposure, a 5 mM concentration of one of the compounds under investigation was applied to the cells. The experimental conditions were meticulously controlled to resemble physiological ones, and all treatments were conducted in an incubator with a steady 37°C temperature and a 5% CO_2 atmosphere. The oxidative stress assay kit employed a redox-based fluorescent probe (SH0403 code) for spectrophotometric assessment. A biological enzyme must hydrolyze diacetyldichlorofluorescein in order to produce fluorescent-green dichlorofluororocein. The generated SH-SY5Y cell lines were given separate doses of DMF (used as a positive control) and H_2O_2 (used as a negative control). The modified cell lines were then exposed to 100 μM chloromethyl derivatives of diacetyldichlorofluorescein for an hour. Fluorescence was specified using a fluorescent microscope, and the reactive oxygen species (ROS) levels were measured in the concerned cell lines using the ROS-detecting kit (code Abcamab 113,851)[94,95].

3.2. Antidiabetic evaluation

The capacity of synthesized DFCs to reduce the enzyme activity of porcine α-amylase and yeast α-glucosidase was assessed using acarbose (ACB) as a reference. Seven sub-solutions were created by distilled water-diluting the parent DMSO solution (2 mg/ml). The concentrations of the created sub-solutions ranged from 1000 to 25 μg/ml. Using the formula (OPD_{ACB}—OPD_{SYN}/OPD_{ACB}) × 100, the percentage of suppression (PS%), a gauge of the antidiabetic effect, was computed for every chemical. Whereas the OPD_{SYN} values were those of the synthetic DFCs, the ACB optical density values were designated as OPD_{ACB}. Nonlinear regression was used to determine the half-maximal inhibitory concentration (IC_{50}) score for each chemical under study. Plotting PS% measurements versus log-scaled concentrations were how this was accomplished. The potency coefficient (PC) of the synthesized DFCs was calculated using the following formula: 1- (IC_{50} of the chemical under investigation - IC_{50} of ACB/IC_{50} of ACB)[96].

3.3. Porcine α-amylase inhibitory assay

A phosphate-buffered solution with a pH of 6.8 was used to dissolve starch, creating a 500 µg/ml substrate solution. At the same time, the enzyme solution was made by mixing 20 µl of it (2 units/ml) with the same amount of the chemical being studied at a known concentration. The 40 µl of the substrate and enzyme solution were then mixed together, and the combination was incubated for 10 minutes at 25°C. The reaction was stopped by adding 0.4 M caustic soda in water, 12% Rochelle salt that has been dried out, and 1% 2-hydroxy-3,5-dinitrobenzoic acid to the mixture that was already moving. The resulting liquid was diluted to 10 ml using distilled water after being heated for 15 minutes in a boiling water bath and cooled to 25°C using tap water. At 540 nm, colorimetric measurement was done to ascertain the chemical's capacity to inhibit the enzyme under study. The blank solution adhered precisely to all the previous steps, apart from substituting distilled water for the inspected solution[97].

3.4. Yeast α-glucosidase inhibitory assay

By dissolving 4-nitrophenol-α-D-glucopyranoside in a phosphate-buffered solution with a pH of 6.8, a 2 ml solution of a 375 µg/ml substrate mixture was created. Simultaneously, 20 µl of glucosidase (0.1 unit/ml) was combined with, in a similar volume, a solution that contained the designated concentration of the chemical being studied to generate the enzyme mixture. The 40 µl substrate mixture and the 40 µl enzyme mixture were then mixed together, and the running mixture was incubated for 30 minutes at 37°C. To stop the reaction, 80 µl of 0.2 M disodium carbonate in buffered solution was added to the mix. At 405 nm, colorimetric analysis was used to find out how well the solution could stop the enzyme from working. The blank solution followed all previous steps exactly, except for adding distilled water in place of the inspected solution[98].

4. Antimicrobial evaluation

4.1. Pathogenic gram-negative aerobes

The broth-dilution method was used to assess the effectiveness of the synthesized DFCs against AG^{-ve} bacterial strains. The growth media utilized was Mueller-Hinton broth (MHB), whereas DMSO was used as a negative control, and ciprofloxacin (Cipro) was used as a positive control. Prior to analysis, 7.5 mg of the chemical under evaluation and 5 ml of DMSO were combined to create the mother solution. After that, autoclaved distilled water was used as a thinning agent to create a series of 13 dilutions. These were labeled appropriately and ranged from 1024 µg/ml to 0.25 µg/ml. In a test tube with a label, 3 ml of MHB, 0.2 ml of inoculant diluted to a 0.5 McFarland standard using autoclaved distilled water, and 1 ml of a preset concentration were combined to create a pre-incubation solution. Following a 24-hour incubation period at 37°C, the samples were visually inspected to evaluate the bacterial growth. The concentration at which the first clear solution was observed represents the first calculated bacteriological index named minimum inhibitory concentrations (MIC). Using diluted amounts based on values of 4, 1, 0.5, or 0.05, depending on the MIC concentration, the earlier methodical steps were repeated to calculate the second bacteriological index known as the minimum bactericidal concentration (MBC). Each compound's final metric, called the potency marker (PM), was calculated by dividing its MBC value by the matching MIC value[99–101].

4.2. Pathogenic anaerobes

Although there were some significant changes, the methodology used to assess the synthesized fused structures' effectiveness against pathogenic ANA bacteria was similar to that used to examine their potential against pathogenic AG^{-ve} bacterial strains. The changes included using metronidazole (Metro) as a positive control and Brucella agar enhanced with 5% sheep blood as a growth medium. Additionally, the incubation period was extended to 48 hours at 37°C in an ANA jar supported by an environment that contained 10% hydrogen, 10% carbon dioxide, and 80% nitrogen. Palladium catalyst and an indicator were used to create this ANA environment [102].

4.3. Pathogenic fungi

The methodology utilized to assess the fungicidal capacity of the synthesized fused structure was similar to that employed to gauge their effectiveness against pathogenic AG^{-ve} bacterial strains. With the exception of the abbreviation MFC, which stands for the minimum fungicidal concentration, the antibacterial characteristics stayed constant. Sabouraud dextrose broth served as the growth medium, and nystatin (Nyst) served as the reference substance. Raising the temperature to 30°C prolonged the incubation period to 48 hours[103].

5. Anti-inflammatory evaluation

In this study, a COX model, including both COX-1 and COX-2 enzymes, was obtained from Cayman (catalog number: 560131) for evaluation. The test compound and the reference drugs (aspirin and celecoxib, which are abbreviated here as Asp and Cxb) were made as a DMSO solution with a concentration of 1 mg/ml. It was then weakened with distilled water until it had a final concentration of between 3.12 and 800 µg/ml. The reaction mixture consisted of 0.96 ml of 0.1 M Tris-HCl buffer, 10 µl of the enzyme preparation, and 100 µl of the test compound. Following a 10-minute incubation at 37°C, arachidonic acid was added to initiate the reaction. Afterward, the mixture was treated with 50 µl of Ellman's reagent (1 M) and allowed to react for 2 minutes. The absorbance was measured spectrophotometrically at 410 nm against a blank control. Based on the obtained data, the IC_{50} values and the COX-1/COX-2 selectivity marker of the test compound were determined[104].

6. Anticancer evaluation

The MTT, 3-[4,5-dimethylthiazol-2-yl]-2,5-diphenyl tetrazolium bromide, assay is used to assess the anticancer potential of the synthesized fused structure. The parent solution for each of the DFCs and the reference medication 5-fluorouracil (5-FU) was prepared as a 1 mg/ml DMSO solution. From this, nine different concentrations: 800, 400, 200, 100, 50, 25, 12.5, 6.25, and 3.12 µg/ml were created by using distilled water as a diluent. AMN-3, HeLa, KYSE-30, MCF-7, SKG, and SK-OV-3 were the six distinct cancer cell lines in which they were also evaluated[105–107]. 10,000 cells from each of the cancer cell lines under investigation were cultivated in each well of a 96-well plate. A day later, different concentrations of the chemical under investigation were given. After 72 hours, the cells' vitality was assessed using a step-by-step protocol that involved removing the medium, adding 28 µl of MTT solution (3.27 mM), and then letting the cells incubate for 90 minutes at 37°C. The microplate reader, which had a 492 nm wavelength set, measured the examined (Ai) and control (Ac) wells' absorbance values. To guarantee precision and optimize effectiveness, this thorough experiment was conducted three times for every chemical under investigation. The growth inhibition percentage (GI%) was calculated using the method $GI\% = [(Ac-Ai)/Ac] \times 100$. Using nonlinear regression, the IC_{50} values might be computed by charting the GI% results against a log-scale concentration gradient[108].

7. Biosafety evaluation

7.1. Non-tumor cells

After the anticancer potential study, biosafety research was done. The first study used an MTT-based visual method to look at how the synthesized fused structures might have helped fight cancer in six different types of tumor cells. The second study investigated the carcinogenicity of these structures using the same first study methodology. But the only difference was the nature of the employed cells, which are non-tumorous ones, including HEK-293 cells, MCF-A10, and RWPE-1[109].

7.2. Commensal bacteria

The biosafety of the synthesized fused structure was tested against commensal bacterial strains using the same broth dilution method that was used to test for pathogenic AG^{-ve} bacterial strains. MHB served as the growth medium, Cipro acted as the positive control, and DMSO functioned as the negative control. The three metric values (MIC, MBC, and PM) were also calculated using the same methodologies[110].

8. Computer-aided pharmaceutical eligibility assessment

8.1. Prediction of *in silico* toxicity

The ProTox-II platform was used to assess the synthetic fused structure's possible toxicity. The toxicity of these compounds would be predicted by looking at their chemical structures and how they match up with the substances in the program dataset. This free platform provides expected details about the toxicity class and potential activity toward the toxicity-mediated enzymes[111].

8.2. Prediction of *in silico* pharmacokinetic parameters

The online prediction tools PreADME and SwissADMET were used to assess the synthetic fused structures' medication compatibility. For research purposes, these publicly available platforms rely on the two-dimensional molecular structure. These websites include a variety of informatics, including water solubility, lipophilicity, bioavailability evaluation, membrane transport mechanism prediction, and other drug-related characteristics[112].

9. Results and discussion

9.1. Synthetic pathway overview

In this study, a systematic, step-by-step synthetic strategy was employed to construct a series of fused heterocyclic compounds (**DFC1**–**DFC7**) with potential pharmacological significance. The approach utilizes key organic reactions, including etherification, condensation, acylation, and functional group modifications, to introduce structural diversity, a crucial aspect for enhancing biological activities. The synthesis begins with the functionalization of 4-chlororesorcinol, which is subjected to etherification using 2-chloroethanol in the presence of triethylamine as a base and ethyl acetate as the solvent. This reaction yields **P-DFC**, an important intermediate bearing both hydroxyl (-OH) and ether (-O-) functionalities, enabling subsequent chemical transformations.

In the subsequent step, the intermediate **P-DFC** undergoes a reaction with 3-ketoglutaric acid under acidic conditions (H2SO4) at low temperatures, yielding **DFC1**. This intermediate introduces key functional groups, such as keto (-CO) and carboxyl (-COOH), which play a vital role in modulating the compound's reactivity and potential biological activity. A pivotal transformation in the synthesis involves converting **DFC1** into its corresponding acyl chloride using thionyl chloride (SOCl2). This step is essential, as acyl chlorides are highly reactive intermediates that facilitate further derivatization, including esterification and amidation. The generated acyl chloride is then subjected to nucleophilic substitution reactions with a series of 4-substituted phenols, namely, 4-methoxyphenol, 4-methylphenol, 4-fluorophenol, 4-chlorophenol, 4-bromophenol, and 4-iodophenol in the presence of pyridine as a mild base. This reaction produces a diverse set of derivatives (**DFC2**–**DFC7**), each featuring distinct substituents that may influence their biological properties. By introducing both electron-donating groups (-OCH3, -CH3) and electron-withdrawing groups (-F, -Cl, -Br, -I), the synthetic strategy allows for a systematic evaluation of electronic effects on pharmacological potential[113].

The DFCs are purified via recrystallization using a mixed solvent system of ether and ethyl acetate, ensuring a high degree of purity. The structural integrity of these compounds is confirmed through a combination of spectroscopic techniques, including IR spectroscopy, NMR, and UV-Vis spectrophotometry.

These analytical tools not only verify the successful formation of the target molecules but also provide comprehensive insights into their molecular architecture. This synthetic approach proves highly effective, offering selective functional group modifications under well-controlled conditions that minimize decomposition and enhance overall yield. Utilizing a common acyl chloride intermediate streamlines the process, enabling the efficient generation of structurally diverse compounds with promising bioactive potential[114].

In conclusion, this methodically engineered synthetic route enables the synthesis of fused heterocyclic derivatives containing pharmacophoric functional groups. The modular design facilitates the development of many analogs, assisting structure activity relationship studies crucial for discovering promising lead compounds with medicinal potential[115].

9.2. Assessment of biological activities

Evaluating the biological activity of new compounds is a crucial phase in drug discovery, agricultural chemistry, and materials research[116]. This procedure facilitates the identification of a compound's medicinal potential, toxicity, and mechanism of action, hence ensuring its safety and efficacy before progressing to subsequent development phases. Biological screening enables researchers to acquire critical insights into the interactions of these compounds with biological targets, hence aiding in the development of more selective and effective molecules[117]. A comprehensive understanding of biological activities can facilitate the creation of novel drugs, insecticides, and bioactive materials with considerable societal and financial significance. In the absence of thorough assessment, advantageous compounds may remain undetected, while potentially detrimental ones could infiltrate the market, endangering both human health and the environment[118].

9.3. Anti-oxidative stress activity

Recent developments in scientific studies on oxidative stress and its connection to several diseases show unequivocally the relationship between oxidative stress and a range of age-related disorders, including cancers, heart diseases, chronic inflammatory diseases, and other health concerns[119]. The intracellular reactive oxygen species (iROS) levels in the human neuroblastoma cell line (SH-SY5Y, ATCC: CRL-2266) exposed to H2O2 under different experimental settings are shown in **Table 1** as relative fluorescence units (RFU). The negative control (cells treated with H2O2) had the greatest iROS level (523.95 RFU), as predicted, demonstrating that exposure to H2O2 causes a considerable amount of oxidative stress. The positive control (DMF), on the other hand, showed a significant decrease in iROS levels (181.45 RFU), indicating that it has substantial antioxidant activity. iROS levels dropped to (211.75 RFU) when H2O2 was given concurrently with DMF (reference condition), confirming DMF's function in reducing oxidative stress. **DFC1** had the highest iROS level (270.10 RFU) of all the chemicals examined (**DFC1**–**DFC7**), suggesting a comparatively weaker antioxidant activity. However, among the test compounds, **DFC4** (188.65 RFU) and **DFC5** (189.90 RFU) had the lowest iROS levels, indicating that their possible antioxidant activity was on par with the reference condition. Conversely, iROS levels were comparatively greater in **DFC6** (255.30 RFU) and **DFC7** (256.50 RFU), suggesting a lesser level of oxidative stress protection. These results imply that whereas some chemicals, like **DFC4** and **DFC5**, might provide protection against oxidative stress, others, including **DFC1**, **DFC6**, and **DFC7**, seem to be less successful. To confirm these results and investigate their possible therapeutic uses in disorders linked to oxidative stress, more investigation is necessary, including dose-response studies and mechanistic analyses.

Table 1. Determining iROS in terms of RFU ± SD (n=3) in H2O2-treated human SH-SY5Y cell line.

Code	Positive control (DMF)	Negative control (H2O2)	Reference (H2O2+DMF)	DFC1
iROS (RFU)	181.45 ± 0.98	523.95 ± 1.08	211.75 ± 0.9	270.10 ± 1.09
Code	**DFC2**	**DFC3**	**DFC4**	**DFC5**
iROS (RFU)	193.80 ± 1.05	209.15 ± 0.89	188.65 ± 0.98	189.90 ± 1.02
Code	**DFC6**		**DFC7**	
iROS (RFU)	255.30 ± 1.12		256.50 ± 0.97	

Further studies are necessary to determine the potential of these DFCs in controlling disorders associated with oxidative stress. At last, the anti-oxidative stress efficacy was arranged in a declining sequence as follows**:** **DFC4**, **DFC5**, **DFC2**, **DFC3**, **DFC6**, **DFC7**, and **DFC1**.

9.4. Antidiabetic activity

Inhibiting α-amylase and α-glucosidase is a critical approach to managing postprandial hyperglycemia in diabetic patients, as they are essential for carbohydrate metabolism and glucose absorption. Although ACB is a potent α-glucosidase inhibitor, its use is frequently accompanied by gastrointestinal adverse effects, underscoring the necessity for alternative inhibitors that exhibit enhanced efficacy and tolerability. In comparison to ACB, **Table 2** offers valuable insights into the inhibitory potential of the DFCs (**DFC1**–**DFC7**) against two critical diabetes-related enzymes, α-amylase and α-glucosidase. The IC50 values, which represent the concentration necessary to inhibit 50% of enzymatic activity, indicate that ACB exhibited the most potent inhibition. The IC50 values for α-amylase were 264.15 µg/ml, and for α-glucosidase, they were 283.85 µg/ml. In contrast, the DFCs exhibited higher IC50 values, which ranged from 287.45 to 327.95 µg/ml for α-amylase and 364.73 to 424.54 µg/ml for α-glucosidase. This suggests that the inhibitory activity of the DFCs was comparatively attenuated.

The sequence of decreasing antidiabetic activity is as follows: **DFC2**, **DFC3**, **DFC1**, **DFC4**, **DFC5**, **DFC6**, and **DFC7**. Furthermore, the higher activity of **DFC2** and **DFC3** may be due to the presence of electron-donating groups, methoxy and methyl, at C-4’ in the molecular frameworks of **DFC2** and **DFC3**, respectively. The increased impact observed may be attributable to the incorporation of these groups into a highly conjugated system, which could potentially enhance the antidiabetic activity. Consequently, **DFC2** and **DFC3** have the potential to be used as prospective lead compounds in the development of effective antidiabetic medications. The derivatives **DFC4**, **DFC5**, **DFC6**, and **DFC7**, which exhibited diminished antidiabetic effectiveness relative to **DFC2** and **DFC3**, may be related to the presence of electron-withdrawing groups (F, Cl, Br, and I) at position 4’ within their molecular structures, along with the integration of these elements into a highly conjugated system, which may significantly reduce the efficacy of their antidiabetic activity. Consequently, modifications in the substituents of the phenyl ring influence the antidiabetic efficacy of the DFCs[120].

Their affinity for target enzymes may be improved through structural modifications, including conjugation strategies or functional group optimization. Furthermore, it will be essential to assess selectivity, bioavailability, and toxicity in order to ascertain their potential as diabetes management drug candidates. Additional investigations, such as molecular docking studies, enzyme kinetics analysis, and *in vivo* evaluations, could offer more profound insights into the therapeutic potential and binding mechanisms of these compounds.

Table 2. The IC50 (µg/ml) ± SD (n=3) and the PF values for ACB and the synthesized fused structures concerning diabetes-related enzymes.

Diabetes-related enzymes	IC50 (µg/ml)							
	Codes of the reference medication and the synthesized fused structures							
	ACB	**DFC1**	**DFC2**	**DFC3**	**DFC4**	**DFC5**	**DFC6**	**DFC7**
α-Amylase	264.15 ± 0.95	306.60 ± 0.98	287.45 ± 1.07	294.70 ± 0.97	311.15 ± 0.99	311.45 ± 0.99	326.10 ± 1.05	327.95 ± 1.08
PF-1	1.00	0.86	0.92	0.90	0.85	0.85	0.81	0.81
α-Glucosidase	283.85 ± 0.92	397.14 ± 1.06	364.73 ± 0.95	367.81 ± 1.09	404.02 ± 1.02	414.35 ± 0.99	422.46 ± 0.98	424.54 ± 1.03
PF-2	1.00	0.84	0.92	0.91	0.83	0.81	0.79	0.79

9.5. Antimicrobial activity

The world is currently dealing with the issue of antibiotic resistance, and occasionally post-operative death cases are reported due to bacterial infections that are resistant to all existing antibiotics, even the most potent ones. To combat different bacterial infections, new antibacterial drugs must be continuously discovered and designed. Derivatives of coumarins have a strong track record of antimicrobial action[110,121–127].

9.5.1. Anti-aerobic gram-negative bacterial strains activity

The antibacterial activity of the DFCs was assessed *in vitro* using the broth dilution method against six AG^{-ve} bacterial strains: *Pseudomonas aeruginosa* (27853-ATCC), *Klebsiella pneumoniae* (700603-ATCC), *Haemophilus influenzae* (49247-ATCC), *Escherichia coli* (25922-ATCC), *Salmonella typhi* (6539-*ATCC)*, and *Shigella dysenteriae* (13313-ATCC). The MIC values of the DFCs, as detailed in **Table 3**, varied from 1.65 to 14.00 µg/ml, and the MBC values ranged from 2.15 to 19.00 µg/ml. The order of diminishing anti-AG^{-ve} bacterial activities is as follows: **DFC5**, **DFC3**, **DFC4**, **DFC2**, **DFC7**, **DFC6**, and **DFC1**. This finding indicated that heightened hydrophobicity of the DFCs correlated with enhanced efficacy against AG^{-ve} bacteria[128]. **DFC5** demonstrated remarkable antibacterial activities against all tested AG^{-ve} bacterial strains, with MIC values of 1.65 µg/ml and MBC values of 2.15 µg/ml. Consequently, it may be regarded as a potential lead molecule warranting additional exploration to enhance its antibacterial efficacy. This may be due to the relatively small size of the chlorine atom at position 4' in **DFC5**, which also functioned effectively as a hydrogen bond acceptor. This could be due to the fact that the para-chlorophenyl unit of **DFC5**, which has both hydrophilic and lipophilic properties, plays a crucial role in the bacteria's ability to penetrate the cell wall and establish a connection with its targets[129,130]. Additionally, **DFC1** exhibited the lowest antibacterial activity among the prepared derivatives. This property may be related to the hydrophilic properties of the acetic acid group in this compound[131]. The PM readings of the DFCs, which ranged from 1.09 to 1.71, were indicative of their capacity to exert bactericidal action against each of the tested AG^{-ve} bacterial strains.

Table 3. The results of the anti-AG^{-ve} efficacy of the reference medication and the synthesized fused structures.

Bacterial strain	Test name	Cipro	DFC1	DFC2	DFC3	DFC4	DFC5	DFC6	DFC7
Escherichia coli	MIC	1.30	14.00	3.45	6.80	6.90	1.65	7.00	6.85
	MBC	1.75	16.00	4.35	8.50	9.25	2.15	7.90	8.50
	PM	1.35	1.14	1.26	1.25	1.34	1.30	1.13	1.24
Haemophilus influenzae	MIC	1.20	14.00	3.60	6.85	6.50	1.75	7.10	6.75
	MBC	1.45	19.00	4.35	9.35	8.40	2.15	8.80	7.65
	PM	1.21	1.36	1.21	1.36	1.23	1.23	1.24	1.13
Klebsiella pneumonia	MIC	0.80	7.00	3.35	3.45	3.45	1.65	7.05	6.95
	MBC	0.95	10.00	5.26	5.10	5.90	2.15	8.80	9.35

Bacterial strain	Test name	Cipro	DFC1	DFC2	DFC3	DFC4	DFC5	DFC6	DFC7
Salmonella typhi	PM	1.19	1.43	1.57	1.48	1.71	1.30	1.25	1.35
	MIC	1.05	14.00	3.55	6.85	6.85	1.90	9.05	8.65
	MBC	1.45	16.00	6.00	8.50	7.55	2.60	10.85	9.45
Shigella dysenteriae	PM	1.38	1.14	1.69	1.24	1.10	1.37	1.20	1.09
	MIC	0.85	14.00	3.75	6.95	3.50	1.80	8.05	7.85
	MBC	1.15	18.00	5.20	8.50	5.15	2.55	8.80	8.65
Pseudomonas aeruginosa	PM	1.35	1.29	1.39	1.22	1.47	1.42	1.09	1.10
	MIC	1.25	14.00	3.55	3.45	3.45	1.70	7.05	6.90
	MBC	1.55	16.00	4.35	4.25	5.05	2.15	7.95	8.50
	PM	1.24	1.14	1.23	1.23	1.46	1.26	1.13	1.23

Table 3. (*Continued*)

The data were presented in terms of μg/ml

9.5.2. Anti-anaerobic bacterial strains activity

The anti-ANA activity of the DFCs was examined against four ANA pathogenic bacterial strains: *Bacteroides fragilis* (25285-ATCC), *Clostridium perfringens* (13124-ATCC), *Fusobacterium necrophorum* (25286-ATCC), and *Prevotella melaninogenica* (25845-ATCC), utilizing the reference drug Metro. **Table 4** presents the antibacterial characteristics of all investigated substances. The reference medication has significantly more bactericidal characteristics than DFCs. The sequence of their antibacterial efficacy was rated in descending order as follows: **DFC2**, **DFC3**, **DFC5**, **DFC4**, **DFC7**, **DFC1**, and **DFC6**. The findings from this study demonstrated considerable anti-ANA efficacy of all the synthesized fused structures, particularly **DFC2**, which exhibited MIC values between 4 and 5 μg/ml and MBC values between 6 and 7 μg/ml. This may be due to the fact that DO ring has a significant role in the anti-ANA activity. These remarkable results facilitate additional investigations to improve these functions, and **DFC2** may serve as a viable lead molecule for further research.

Table 4. The results of the anti-ANA efficacy of the reference medication and the synthesized fused structures.

Bacterial strain	Antimicrobial parameter	Codes of the reference medication and the synthesized fused structures							
		Metro	DFC1	DFC2	DFC3	DFC4	DFC5	DFC6	DFC7
Bacteroides fragilis	MIC	3.55	32.00	5.00	8.00	22.00	20.00	33.00	28.00
	MBC	3.95	46.00	7.00	13.00	25.00	27.00	51.00	41.00
	PM	1.11	1.44	1.40	1.63	1.14	1.35	1.55	1.46
Clostridium perfringens	MIC	1.15	29.00	4.00	6.00	20.00	18.00	30.00	18.00
	MBC	1.75	42.00	6.00	9.00	25.00	24.00	44.00	25.00
	PM	1.52	1.45	1.50	1.50	1.25	1.33	1.47	1.39
Fusobacterium necrophorum	MIC	1.95	19.00	4.00	6.00	23.00	17.00	24.00	22.00
	MBC	2.15	25.00	7.00	10.00	33.00	21.00	34.00	31.00
	PM	1.10	1.32	1.75	1.67	1.43	1.24	1.42	1.41
Prevotella melaninogenica	MIC	1.05	26.00	5.00	6.00	26.00	23.00	27.00	27.00
	MBC	1.55	42.00	7.00	10.00	36.00	30.00	41.00	41.00
	PM	1.48	1.62	1.40	1.67	1.38	1.30	1.52	1.52

The data were presented in terms of μg/ml

9.5.3. Anti-fungal activity

The synthesized fused structures were evaluated for their antifungal activity against two fungus strains, *Candida albicans* (10231-ATCC) and *Aspergillus niger* (16888-ATCC), using the antifungal agent Nyst as a reference. The results presented in **Table 5** indicate the antimicrobial parameters for all tested DFCs. The prepared derivatives exhibited a diverse pattern of fungal suppression activity against the tested fungi, with MIC and MFC values ranging from 0.95 to 25.00 µg/ml and from 1.20 to 28.00 µg/ml, respectively. **DFC1**, **DFC2**, **DFC3**, **DFC4**, and **DFC5** exhibited significant antifungal efficacy that exceeded the reference, with **DFC1** displaying somewhat greater antifungal activity than **DFC2**, **DFC3**, **DFC4**, and **DFC5**, which possess para-substituted phenol rings with methoxy, methyl, fluorine, and chlorine, respectively. The findings underscore the significant importance of DO ring in the antifungal efficacy of DFCs. The bromo- and iodo-substituted phenol conjugates (**DFC6** and **DFC7**) had the least antifungal efficacy among the compounds tested.

Table 5. The results of the antifungal efficacy of the reference medication and the synthesized fused structures.

Fungal strain	Antimicrobial parameter	Codes of the reference medication and the synthesized fused structures							
		Nyst	**DFC1**	**DFC2**	**DFC3**	**DFC4**	**DFC5**	**DFC6**	**DFC7**
Candida albicans	MIC	4.00	0.95	3.50	3.50	1.15	1.25	14.00	13.00
	MFC	7.00	1.25	4.50	5.00	1.25	1.50	15.00	14.00
	PM	1.75	1.32	1.29	1.43	1.09	1.20	1.07	1.08
Aspergillus niger	MIC	9.00	1.00	8.00	9.00	1.45	1.50	24.00	25.00
	MFC	11.00	1.20	9.50	11.00	2.00	1.75	25.00	28.00
	PM	1.22	1.20	1.19	1.22	1.38	1.17	1.04	1.12

The data were presented in terms of µg/ml

Table 6. The IC_{50} (µg/ml) ± SD (n = 3) values for aspirin, celecoxib, and the synthesized fused structures against inflammation related enzymes.

Inflammation related enzymes	IC50 (µg/ml)								
	Codes of the reference medication and the synthesized annulates								
	Aspirin	**Celecoxib**	**DFC1**	**DFC2**	**DFC3**	**DFC4**	**DFC5**	**DFC6**	**DFC7**
COX-1	3.78 ± 0.98	7.68 ± 1.06	97.49 ± 0.97	153.96 ± 0.99	153.73 ± 0.96	146.35 ± 1.01	146.93 ± 1.03	175.18 ± 0.92	175.93 ± 1.06
COX-2	30.12 ± 1.04	1.65 ± 1.12	74.52 ± 1.03	117.13 ± 1.05	117.18 ± 1.02	94.85 ± 1.07	103.30 ± 1.09	136.19 ± 0.99	138.87 ± 1.12
COX-1/COX-2 selectivity	0.13	4.65	1.31	1.31	1.31	1.54	1.42	1.29	1.27

9.6. Anti-inflammatory activity

The anti-inflammatory activity of the reference medications, Asp and Cxb, alongside the newly synthesized fused structures (**DFC1**–**DFC7**), was evaluated by examining their inhibitory effects on two critical enzymes implicated in inflammation: COX-1 and COX-2. **Table 6** presents the IC_{50} values obtained from the reference agents and DFCs. Asp demonstrated potent COX-1 inhibition, with an IC_{50} of 3.78 µg/ml, but its impact on COX-2 was markedly diminished (IC_{50} = 30.12 µg/ml), yielding a COX-1/COX-2 selectivity ratio of 0.13, thereby affirming its predilection for COX-1. Cxb, a recognized COX-2 selective inhibitor, had an IC_{50} of 7.68 µg/ml for COX-1 and a significantly lower IC_{50} of 1.65 µg/ml for COX-2, resulting in a selectivity ratio of 4.65, underscoring its pronounced preference for COX-2.

Among the synthesized compounds, **DFC1** to **DFC7** demonstrated differing levels of COX enzyme inhibition. **DFC1** exhibited moderate selectivity for COX-2, with IC_{50} values of 97.49 µg/ml for COX-1 and 74.52 µg/ml for COX-2, resulting in a selectivity ratio of 1.31. Likewise, **DFC2** and **DFC3** exhibited similar

IC_{50} values (153.96 and 153.73 μg/ml for COX-1, and 117.13 and 117.18 μg/ml for COX-2, respectively), both preserving a COX-1/COX-2 selectivity ratio of 1.31. **DFC4** and **DFC5** demonstrated somewhat greater selectivity for COX-2, with selectivity ratios of 1.54 and 1.42, respectively. Simultaneously, **DFC6** and **DFC7** exhibited the highest IC_{50} values among the synthetic compounds, with COX-1 IC_{50} values of 175.18 and 175.93 μg/ml, and COX-2 IC_{50} values of 136.19 and 138.87 μg/ml, respectively, resulting in selectivity ratios of 1.29 and 1.27. Cxb was identified as the most selective COX-2 inhibitor, whereas Asp largely exhibited COX-1 selectivity. DFCs had considerable COX-2 selectivity, with **DFC4** showing the most preference among them. The finding indicate that DFCs possesses promise for the creation of anti-inflammatory drugs with enhanced COX-2 selectivity, presenting exciting

9.7. Anti-cancer activity

The anticancer activity of the DFCs was assessed *in vitro* utilizing an MTT assay against six cancer cell boundaries: AMN3 (murine mammary adenocarcinoma, CVCLM395), HeLa (epithelioid cervix cancer, 93021013), KYSE-30 (human Asian esophageal squamous cell cancer, 94072011), MCF-7 (human breast carcinoma), SKG (human papillomavirus-related cervical squamous cell cancer, C27676), and SK-OV-3 (Caucasian ovary adenocarcinoma, 91091004), with 5-FU serving as a reference chemotherapeutic agent. **Table 7** displays the IC50 values (μg/ml) of 5-FU and a selection of DFCs against the examined cancer cell lines. The IC50 value denotes the concentration of a substance necessary to diminish cell viability by 50%, serving as a critical metric for evaluating anticancer efficacy. A diminished IC50 value signifies enhanced cytotoxic efficacy, while elevated values indicate less activity against cancer cells.

Among the evaluated cell lines, 5-FU consistently exhibited the lowest IC50 values, highlighting its potent anticancer efficacy. It demonstrated IC50 values of 13.40 μg/ml for HeLa (cervical cancer) and 12.55 μg/ml for MCF-7 (breast cancer), which were markedly lower than those of the majority of DFCs. Nonetheless, several fused structures, like **DFC4**, exhibited notable cytotoxic efficacy, especially against MCF-7 and HeLa cells, with IC50 values nearing those of 5-FU. This significant effect may be related to the fluoro group's attachment to position 4' in the **DFC4** framework formula[132]. Numerous studies emphasize the beneficial effects of fluoride substitution in the compound's aromatic system with regard to its ability to prevent proliferation. Additionally, as a hydrogen-bond acceptor, the fluoro groups can participate in interactions between the molecule and the target[133–135].

In contrast, certain chemicals like **DFC1** demonstrated the lowest potency among all evaluated cell lines, indicating diminished anticancer efficacy, with IC_{50} values of 85.13 μg/ml for SKG and 76.07 μg/ml for MCF-7. This finding might be linked to the acetic acid group in the structure of **DFC1**, which makes it very water-attracting, increasing its hydrophilic properties and reducing its ability to enter cancer cells[136–139]. This suggests the necessity for additional structural alterations to improve its therapeutic efficacy. The effectiveness of the synthesized fused structures against cancer varies in the different cell lines because of the differences in how these compounds are structured. **DFC4** shows the highest anticancer activity for all the examined cancer cell lines; this property may be due to the fluoro substitution in the framework of the compound.

The disparity in IC50 values across several cancer cell lines underscores the selective characteristics of the produced drugs. Some compounds worked better on specific cancer cells, especially **DFC2**, which was very effective against MCF-7 (20.90 μg/ml) and KYSE-30 (38.87 μg/ml), suggesting they could be used for personalized cancer treatment. Conversely, others like **DFC7** demonstrated persistently elevated IC50 values across many cell lines, signifying restricted anticancer effectiveness. In conclusion, although 5-FU is the most effective molecule assessed, certain DFCs exhibit promising anticancer efficacy, especially against particular cancer types. Changing their structure or combining them with other treatments could make these compounds work better and target cancer more effectively, improving their use in therapy.

Table 7. IC50 (µg/ml) ± SD (n=3) values for 5-FU and the synthesized fused structures against the assessed cancer cell lines.

Cancer cell lines	IC50 (µg/ml)							
	Codes of the reference medication and the synthesized fused structures							
	5-FU	**DFC1**	**DFC2**	**DFC3**	**DFC4**	**DFC5**	**DFC6**	**DFC7**
AMN-3	25.15 ± 1.05	52.23 ± 1.11	44.74 ± 0.91	56.15 ± 0.99	25.93 ± 0.95	27.77 ± 1.01	51.70 ± 1.03	56.81 ± 0.97
HeLa	13.40 ± 1.11	51.15 ± 1.08	17.58 ± 1.00	32.42 ± 0.90	13.13 ± 0.98	15.73 ± 1.03	43.81 ± 0.98	44.48 ± 1.06
KYSE-30	31.25 ± 1.02	53.06 ± 0.97	38.87 ± 1.11	41.68 ± 1.07	34.99 ± 0.99	35.09 ± 1.15	43.97 ± 1.14	46.14 ± 1.07
MCF-7	12.55 ± 1.07	76.07 ± 1.03	20.90 ± 1.13	25.87 ± 0.98	12.57 ± 1.13	21.00 ± 1.13	70.33 ± 0.93	74.51 ± 1.06
SKG	22.45 ± 1.10	85.13 ± 0.19	37.31 ± 1.10	33.60 ± 1.15	29.20 ± 1.05	29.28 ± 0.98	70.29 ± 0.97	67.34 ± 1.06
SK-OV-3	22.90 ± 1.08	52.01 ± 0.99	47.16 ± 1.05	31.78 ± 0.95	22.23 ± 0.92	25.43 ± 0.93	45.93 ± 1.07	50.82 ± 1.01

10. Biocompatible measures

10.1. Biosafety toward noncancerous cells

The biosafety evaluation of the synthesized fused structures, relative to the commonly utilized chemotherapeutic drug 5-FU, offers critical insights into their lethal effects on non-tumor cell lines. This assessment relies on IC50 values, which denote the concentration necessary to reduce cell proliferation by 50%, functioning as a critical metric of cytotoxicity. The research investigates three non-tumor cell lines: HEK-293 (human embryonic kidney cells), MCF-10A (non-tumorigenic breast epithelial cells), and RWPE-1 (normal prostate epithelial cells).

In **Table 8**, 5-FU in all three cell lines exhibits reduced IC50 values, indicating increased toxicity to healthy cells. 5-FU has an IC50 of 39.65 µg/ml in HEK-293 cells, while the DFCs have significantly higher IC50 values, with **DFC4** displaying the lowest cytotoxicity at 206.10 µg/ml. A comparable trend is shown in MCF-10A cells, with 5-FU exhibiting an IC50 of 40.55 µg/ml, whereas the produced compounds vary from 81.10 µg/ml to 231.25 µg/ml, signifying reduced toxicity. In RWPE-1 cells, 5-FU demonstrates the lowest IC50 at 33.25 µg/ml, but **DFC4** is the least hazardous, exhibiting an IC50 of 205.20 µg/ml. The order of lowering the biosafety effect is **DFC4**, **DFC5**, **DFC2**, **DFC3**, **DFC6**, **DFC7**, and **DFC1**.

The results indicate that the synthesized DFCs demonstrates markedly reduced toxicity to non-tumor cell lines in comparison to 5-FU, an advantageous trait for prospective therapeutic advancement. Elevated IC50 values signify that larger doses of the chemicals are required to elicit lethal effects, indicating a more advantageous biosafety profile. Significantly, **DFC4** consistently demonstrates the greatest IC50 values among all evaluated cell lines, indicating it may be the least detrimental to healthy cells. This characteristic renders **DFC4** a compelling prospect for further exploration in drug development, perhaps providing a more selective and safer method for cancer treatment.

Table 8. IC50 (µg/ml) ± SD (n = 3) values for 5-FU and the synthesized fused structures against the assessed non-tumor cell lines.

Non-tumor cell lines	IC50 (µg/ml)							
	Codes of the reference medication and the synthesized fused structures							
	5-FU	**DFC1**	**DFC2**	**DFC3**	**DFC4**	**DFC5**	**DFC6**	**DFC7**
HEK-293	39.65 ± 1.18	75.50 ± 1.01	102.90 ± 1.08	91.15 ± 0.99	206.10 ± 0.97	100.95± 1.15	81.80 ± 1.03	70.75 ± 1.23
MCF-A10	40.55± 0.94	81.10 ± 1.09	108.85 ± 1.15	95.85 ± 1.05	231.25 ± 1.04	111.15± 0.99	88.85 ± 1.01	82.50 ± 1.08
RWPE-1	33.25 ± 1.11	71.55 ± 1.09	98.90 ± 1.17	86.25 ± 0.99	205.20 ± 1.02	103.80± 1.19	78.75 ± 1.02	72.30 ± 0.99

10.2. Biosafety toward commensal bacterial strains

Nearly all prescribed medications, especially oral ones, adversely affect the normal development of the gut microbiota and may lead to side effects, including diarrhea[140]. To evaluate the validity of this notion about the synthesized DFCs, we examined their impact on the proliferation of normal microbiota utilizing three strains of commensal bacteria: *Escherichia coli* (BAA-1427), *Escherichia coli* (MG1655), and *Escherichia coli* (BAA1430). This assessment utilized Cipro as a reference agent because it is an officially approved orally supplied medicine, and it ensures the technique's efficacy[141]. The antibacterial properties assessed for the synthetic DFCs and Cipro are presented in **Table 9**.

The toxicity order of these compounds, from least to most poisonous, is as follows: **DFC5**, **DFC4**, **DFC3**, **DFC1**, **DFC7**, **DFC6**, and **DFC2**. Cipro markedly impeded the normal development of the assessed commensal bacteriomes. Furthermore, the synthetic compounds, especially **DFC5**, exhibited an antibacterial efficacy much lower than that of Cipro against the assessed commensal bacteriomes. All analyzed structures demonstrated bactericidal properties, as indicated by their low PM values, raising concerns about their biosafety qualities. Therefore, additional thorough examinations are essential to confirm their safety[142].

Table 9. Biosafety results of the reference medication and the synthesized fused structures toward the assessed commensal bacteriomes.

Bacterial strain	Antimicrobial parameters	Codes of the reference medication and the synthesized fused structures							
		Cipro	DFC1	DFC2	DFC3	DFC4	DFC5	DFC6	DFC7
Escherichia coli (BAA-1427)	MIC	1.05	17.00	11.00	18.00	19.00	28.00	14.00	14.00
	MBC	1.75	21.00	18.00	27.00	25.00	47.00	20.00	21.00
	PM	1.67	1.22	1.65	1.52	1.30	1.67	1.39	1.49
Escherichia coli (MG1655)	MIC	1.75	19.00	18.00	29.00	34.00	43.00	14.00	16.00
	MBC	2.30	22.00	25.00	40.00	42.00	68.00	21.00	21.00
	PM	1.31	1.16	1.37	1.39	1.22	1.57	1.49	1.30
Escherichia coli (BAA1430)	MIC	1.15	12.00	18.00	26.00	32.00	37.00	16.00	17.00
	MBC	1.95	18.00	29.00	36.00	42.00	52.00	25.00	23.00
	PM	1.70	1.52	1.59	1.40	1.30	1.41	1.54	1.38

The data were presented in terms of μg/ml

11. Computer-aided pharmacological eligibility evaluation

11.1. Expected in silico toxicity profile

A principal obstacle hindering the advancement and accessibility of numerous studies in the applied medical field was the potential toxicity of specific synthetic compounds[143]. Numerous computer-aided systems have been created to predict the probable toxicity of various synthetic compounds[144]. This study employed the ProTox-II platform to predict the toxicity profile of the synthesized DFCs. The toxicity-related terminology derived from this platform is described in **Table 10**. This toxicity profile provides a comparative analysis of seven novel synthetic compounds, designated **DFC1** to **DFC7**, assessed across various critical toxicological parameters.

We uniformly designate all chemicals with an expected toxicity level of 4, which signifies a consistent forecast of overall toxicity, regardless of structural variations. This homogeneity indicates that these substances may possess analogous toxicophoric traits that influence their similar risk profiles. Carcinogenicity probabilities range between 0.50 and 0.55, indicating a modest potential for carcinogenic consequences. Among the chemicals, **DFC2** demonstrates the highest predicted carcinogenicity (0.55), whereas **DFC6** shows the lowest (0.50), indicating only slight variations in their potential cancer risk. Cytotoxicity readings range

from 0.72 to 0.85, which is a somewhat increased range. Notably, **DFC4** and **DFC5** had lower scores (0.72), suggesting a comparatively lower cytotoxic potential, while **DFC2** and **DFC3** exhibit the highest cytotoxicity (0.85), suggesting a larger risk of causing cellular damage.

The predictions for immunogenicity vary significantly, ranging from 0.78 to 0.99. **DFC1** has a high potential to elicit immunological responses, as evidenced by its greatest likelihood (0.99). High scores for **DFC3** (0.97) and **DFC7** (0.95) further emphasize the necessity of a thorough immune-toxicological assessment of these substances. Liver toxicity projections vary from 0.65 to 0.85, with **DFC1** demonstrating the highest value of 0.85, indicating an elevated risk of hepatotoxicity. Conversely, **DFC5** has a diminished score of 0.65, signifying a comparatively decreased likelihood of liver-related adverse effects. Mutagenicity ranges from 0.67 to 0.78, with **DFC1** consistently identified as the chemical with the highest anticipated risk of 0.78, signifying a comparatively high risk of mutagenicity. Conversely, **DFC6** has a diminished score of 0.67, indicating a decreased likelihood of mutagenicity adverse effects. The small range across all compounds indicates a mild worry regarding mutagenesis potential, with minimal heterogeneity among structures[145].

In conclusion, **DFC1** continuously exhibits the highest risk across all toxicological endpoints, especially in immunogenicity, hepatotoxicity, and mutagenicity, rendering it the most potentially perilous choice within the cohort. Conversely, **DFC5** and **DFC6** have relatively reduced toxicity values in multiple domains, indicating a more advantageous safety profile. These insights are useful in directing the prioritization of compounds for subsequent research or structural enhancement.

Table 10. Toxicological characteristics of the synthesized fused structures

Toxicity- related terms	Codes of the synthesized fused structures						
	DFC1	**DFC2**	**DFC3**	**DFC4**	**DFC5**	**DFC6**	**DFC7**
A-Tox-level	4	4	4	4	4	4	4
Car-Tox (P)	0.53	0.55	0.54	0.52	0.53	0.50	0.52
Cyt-Tox (P)	0.77	0.85	0.85	0.72	0.72	0.74	0.74
Imm-Tox (P)	0.99	0.81	0.97	0.78	0.87	0.81	0.95
Liver-Tox (P)	0.85	0.80	0.80	0.67	0.65	0.67	0.67
Mut-Tox (P)	0.78	0.75	0.75	0.68	0.68	0.67	0.68

A-Tox-level: Anticipated toxicity level, Car-Tox: Carcinogenicity, Cyt-Tox: Cytotoxicity, Imm-Tox: Immunogenicity, Liver-Tox: Liver toxicity, and Mut-Tox: Mutagenicity.

11.2. Expected in silico pharmacokinetic profile

The assessment of pharmacokinetic parameters in drug candidates presents a significant challenge and serves as a critical hurdle in lead compound selection and drug development. One of the primary reasons for drug candidate failure during development is poor ADME (Absorption, Distribution, Metabolism, and Excretion) characteristics, which account for nearly half of all setbacks. To mitigate this issue, *in silico* approaches have been widely employed to predict ADME properties, providing valuable guidance in the early stages of drug discovery. These computational tools help in identifying promising lead compounds before proceeding to *in vitro* and *in vivo* evaluations, ultimately saving time and resources[146].

In this study, the pharmacokinetic properties of the DFCs were evaluated using SwissADME and preADMET, with key findings summarized in **Table 11**. Except for **DFC1** and **DFC2**, which have no penetration characteristics, all DFCs were able to pass across the blood–brain barrier. During the design phase, brain penetration is a crucial consideration for any attempt to target or avoid the brain. The potential for detrimental CNS side effects is reduced or eliminated by compounds' blood–brain barrier impermeability[147,148].

The results revealed that DFCs exhibited moderate permeability in the Caco-2 cell model and high human intestinal absorption, ranging from 90.88% to 99.00%. These findings suggest that intestinal absorption may involve mechanisms beyond simple passive diffusion[149]. The Caco-2 cell model, while widely used for permeability studies, has certain limitations, such as the absence of mucus-secreting cells, transport proteins, and other physiological factors like phospholipids and bile acids, all of which can influence absorption. Furthermore, the presence of tight junctions in Caco-2 cells restricts paracellular transport, potentially reducing the permeability of certain compounds. These factors should be considered when interpreting *in vitro* permeability data in the context of drug absorption predictions[150,151].

Additionally, except for **DFC1**, all DFCs blocked the CYP3A4 enzyme, which breaks down and eliminates about 50% of marketed medications. A drug-drug interaction will occur as a result of this enzyme inhibition[152,153]. Furthermore, with the exception of **DFC1**, the synthetic DFCs inhibited the CYP2C9 enzyme, which may lead to drug interactions with other medications that use this enzyme for metabolism[154–156]. In contrast, these compounds did not inhibit the CYP2D6 enzyme except for **DFC2**, and there is very little chance of drug-drug interactions between these compounds and the drugs metabolized by this enzyme[157,158].

The Lipinski Rule of Five is a widely used guideline for assessing the drug-likeness of orally administered compounds. According to this rule, a molecule is more likely to be orally bioavailable if it meets the following criteria: no more than 10 hydrogen bond acceptors, no more than 5 hydrogen bond donors, a log P value of 5 or lower (indicating balanced lipophilicity), and a molecular weight not exceeding 500 Daltons[159–161]. A compound can still be considered suitable for oral delivery if it violates only one of these conditions; otherwise, poor absorption and bioavailability may be expected. Based on *in silico* analysis, all DFCs comply with Lipinski's criteria, suggesting they have a high potential for successful development. Their favorable physicochemical properties reduce the likelihood of failure during drug discovery and clinical trials, increasing their chances of commercialization[162,163].

Moreover, **DFC1-DFC7** derivatives inhibited the P-glycoprotein transporter. They can therefore increase the apical-to-basolateral intestinal permeability and bioavailability of drugs that act as this efflux mechanism's substrates. Furthermore, the inhibition of the P-glycoprotein transporter may be the cause of several drug-drug interactions that took place throughout the distribution and elimination processes[164,165].

Furthermore, except for **DFC1**, which showed low plasma protein binding capabilities, the synthetic DFCs had high plasma protein binding capabilities, ranging from 86.18 to 98.39%. This resulted in a reduced volume of distribution, a prolonged plasma half-life, and a restricted clearance rate. High plasma protein binding ability may potentially affect efficacy because pharmacological action is only ascribed to the drug's free fraction[166–168].

The projected water solubility of the seven DFCs compounds ranges from 5.10 mg/mL for **DFC4** to 9.86 mg/mL for **DFC1**. All compounds demonstrate moderate aqueous solubility, which is beneficial for oral medication administration and formulation development. **DFC1** exhibits the highest solubility, suggesting it may possess enhanced dissolving and absorption properties. Conversely, **DFC4** exhibits the lowest solubility, potentially complicating bioavailability unless mitigated by formulation techniques, including the incorporation of solubilizing agents or nanocarriers[169–171].

Concerning synthetic feasibility, the chemicals exhibit scores between 2.95 (**DFC1**) and 3.51 (**DFC2**), indicating they are predominantly attainable for synthesis. The scores derive from cheminformatics assessments of molecular complexity, functional group presence, and predicted synthetic steps required. Reduced synthetic feasibility values indicate simpler synthesis[172]. **DFC1**, with the highest solubility and the lowest synthetic feasibility score, seems very promising for subsequent development. Despite **DFC2** and **DFC7** exhibiting marginally elevated values of 3.51 and 3.49, respectively, they are still within a range deemed tolerable in medicinal chemistry.

In conclusion, all DFCs compounds exhibit a beneficial balance between water solubility and synthetic feasibility, with **DFC1** identified as a prominent lead contender owing to its desirable activities of high solubility and straightforward synthesis[173–175].

Table 11. Pharmacokinetic properties of the synthesized fused structures as projected by open access platforms.

Pharmacokinetic parameters	Codes of the synthesized fused structures						
	DFC1	**DFC2**	**DFC3**	**DFC4**	**DFC5**	**DFC6**	**DFC7**
BBB	No	No	Yes	Yes	Yes	Yes	Yes
CCP	20.71	45.76	46.20	40.99	28.55	26.47	26.34
CYP3A4	No	Yes	Yes	Yes	Yes	Yes	Yes
CYP2C9	No	Yes	Yes	Yes	Yes	Yes	Yes
CYP2D6	No	Yes	No	No	No	No	No
Bio-A	0.56	0.55	0.55	0.55	0.55	0.55	0.55
IA%	90.88	99.00	98.81	98.84	98.39	97.90	97.96
LR-5	Suitable	Suitable	Suitable	Suitable	Suitable	Suitable	Suitable
P-gp	No	No	No	No	No	No	No
PPB	51.21	86.18	89.21	88.07	90.03	91.10	98.39
PWS	9.86	5.83	8.85	5.10	5.72	9.55	5.76
SF	2.95	3.51	3.47	3.33	3.33	3.36	3.49

BBB: Ability to cross the blood brain barrier, CCP: Caco 2 cell permeability in nm/sec, CYP: Cytochrome-P450, Bio-A: Bioavailability, IA%: Percentage of intestinal drug absorption, LR-5 Lipinski's rule of five, P-gp: Ability to bypass the glycoprotein pumping, PPB: Extent of plasma protein binding, PWS: Predicted water solubility in mg/ml, SF: Synthetic feasibility.

12. Conclusion

In this study, seven novel synthetic DFC compounds were successfully synthesized and thoroughly characterized. Comprehensive experimental and computational analyses revealed several key findings: First, **DFC4** demonstrated the highest antioxidant capacity, effectively counteracting oxidative stress. This suggests its potential role in preventing oxidative damage-related diseases. Second, the presence of electron-donating groups, such as methoxy and methyl at C-4', significantly enhanced the antidiabetic activity of **DFC2** and **DFC3**. These structural modifications appear to contribute to improved glucose regulation, highlighting their potential in diabetes management. Third, **DFC5** exhibited broad-spectrum antibacterial activity against all tested AG^{-ve} bacterial strains, with potency comparable to Cipro. Notably, **DFC5** also displayed a superior biosafety profile, being significantly less disruptive to beneficial commensal bacteria than Cipro. Fourth, **DFC2** was identified as the most effective against ANA bacterial strains, further expanding the antimicrobial spectrum of these compounds. Fifth, **DFC1** also demonstrated strong antifungal activity, surpassing that of Nyst. This highlights the impact of its heterocyclic structure in enhancing antifungal potency. Sixth, **DFC1** exhibited the most pronounced anti-inflammatory effects among the tested compounds, suggesting its potential as an effective anti-inflammatory agent. Seventh, **DFC4** displayed potent anticancer activity, showing even greater efficacy than 5-FU against certain cancer cell lines. Regarding biosafety, **DFC4** exhibited the lowest toxicity toward non-tumor cell lines, indicating its selective cytotoxicity against cancer cells while preserving normal cell viability. The tested DFC compounds demonstrated minimal toxicity toward commensal microbiota, suggesting their potential for safe therapeutic use without significantly disrupting normal bacterial populations, with **DFC5** standing out as the least toxic to commensal microbiota. Finally, pharmacokinetic evaluations using predictive web-based tools indicated that the synthetic compounds possess favorable drug-like properties, making them promising candidates for future oral drug formulations. Given these findings, the

new DFC compounds hold significant potential as broad-spectrum antimicrobials, anti-inflammatories, and anticancer agents, paving the way for further pharmaceutical exploration.

Conflict of interest

The authors declare no conflict of interest.

About the author

Marwa Mohammed Alshaher, marwa.23php33@student.uomosul.edu.iq , http://orcid.org/0009-0006-9647-1780;

Yasser Fakri Mustafa, http://orcid.org/0000-0002-0926-7428

References

1. Al-Jumaili MHA, Hamad AA, Hashem HE, Hussein AD, Muhaidi MJ, Ahmed MA, ALBANAA AHA, Siddique F, Bakr EA. Comprehensive review on the Bis–heterocyclic compounds and their anticancer efficacy. Journal of Molecular Structure. 2023;1271:133970.
2. Ahmed K, Choudhary MI, Saleem RSZ. Heterocyclic pyrimidine derivatives as promising antibacterial agents. European Journal of Medicinal Chemistry. 2023;259:115701.
3. Subramani Karthikeyan Maria Grishina SKRMARSCGNP, Kennedy LJ. A review on medicinally important heterocyclic compounds and importance of biophysical approach of underlying the insight mechanism in biological environment. Journal of Biomolecular Structure and Dynamics. 2023;41(23):14599–619.
4. Venugopala KN, Rashmi V, Odhav B. Review on natural coumarin lead compounds for their pharmacological activity. BioMed Research International. 2013;2013.
5. Oglah MK, Kahtan Bashir M, Fakri Mustafa Y, Mohammed ET, Khalil RR. Synthesis and biological activities of 3,5-disubstituted-4-hydroxycinnamic acids linked to a functionalized coumarin. Systematic Review Pharmacy. 2020;11(6):717–25.
6. Mustafa YF. Coumarins derived from natural methoxystilbene as oxidative stress-related disease alleviators: Synthesis and in vitro-in silico study. Journal of Molecular Structure. 2024;1302:137471.
7. Younes AH, Mustafa YF. Novel coumarins from green sweet bell pepper seeds: Their isolation, characterization, oxidative stress-mitigating, anticancer, anti-inflammatory, and antidiabetic properties. Journal of Molecular Structure. 2024;1312:138629.
8. Reddy DS, Kongot M, Singh V, Maurya N, Patel R, Kumar Singhal N, Avecilla F, Kumar A. Coumarin tethered cyclic imides as efficacious glucose uptake agents and investigation of hit candidate to probe its binding mechanism with human serum albumin. Bioorganic Chemistry. 2019;92:103212.
9. Jebir RM, Mustafa YF. Watermelon Allsweet: A promising natural source of bioactive products. Journal of Medicinal and Chemical Sciences. 2022;5(5):652–66.
10. Mustafa YF. Effects of heat variables on the starch content of cooked white rice: Searching for diabetes-friendly food. Bioactive Carbohydrates and Dietary Fibre. 2024;31:100395.
11. Annunziata F, Pinna C, Dallavalle S, Tamborini L, Pinto A. An overview of coumarin as a versatile and readily accessible scaffold with broad-ranging biological activities. International Journal of Molecular Sciences. 2020;21(13):1–83.
12. Mustafa YF. Synthesis, characterization and antibacterial activity of novel heterocycle, coumacine, and two of its derivatives. Saudi pharmaceutical journal. 2018;26(6):870–5.
13. Mustafaa YF. New Coumarin-Metronidazole Composites: Synthesis, Biocompatibility, and Anti-anaerobic Bacterial Activity. Russian Journal of Bioorganic Chemistry. 2024;50(1):201–10.
14. Satyanarayana VSV, Sreevani P, Sivakumar A, Vijayakumar V. Synthesis and antimicrobial activity of new Schiff bases containing coumarin moiety and their spectral characterization. Arkivoc. 2008;2008(17):221–33.
15. Mohammed ET, Khalil RR, Mustafa YF. Phytochemical Analysis and Antimicrobial Evaluation of Quince Seeds' Extracts. Journal of Medicinal and Chemical Sciences. 2022;5(6):968–79.
16. Abdulaziz NT, Mustafa YF. The Effect of Heat Variable on the Chemical Composition and Bioactivities of a Citrullus lanatus Seed Aqueous Extracts. Journal of Medicinal and Chemical Sciences. 2022;5(7):1166–76.
17. Mustafa YF. Coumarins from carcinogenic phenol: synthesis, characterization, in silico, biosafety, anticancer, antioxidant, and anti-inflammatory assessments. Chemical Papers. 2024;78:493–504.
18. Mustafa YF. Combretastatin A4-based coumarins: synthesis, anticancer, oxidative stress-relieving, anti-inflammatory, biosafety, and in silico analysis. Chemical Papers. 2024;78:3705–3720.
19. Younes AH, Mustafa YF. Unveiling the Biomedical Applications of Novel Coumarins Isolated From Capsicum Annuum L. Seeds by a Multivariate Extraction Technique. Chemistry and Biodiversity. 2024;21(6):e202400581.

20. Oglah MK, Mustafa YF. Synthesis, antioxidant, and preliminary antitumor activities of new curcumin analogues. Journal of Global Pharma Technology. 2020;12(2):854–62.
21. Mustafa YF, Oglah MK, Bashir MK, Mohammed ET, Khalil RR. Mutual prodrug of 5-ethynyluracil and 5-fluorouracil: Synthesis and pharmacokinetic profile. Clinical Schizophrenia and Related Psychoses. 2021;15(5):1–6.
22. Mustafa YF. Nutraceutical-based telomerase inhibitors: Renewed hope for cancer therapy. Phytomedicine Plus. 2024;4(2):100537.
23. Pereira TM, Franco DP, Vitorio F, Kummerle AE. Coumarin compounds in medicinal chemistry: Some important examples from the last years. Current Topics in Medicinal Chemistry. 2018;18(2):124–48.
24. Molnar M, Amic A, Pavic V, Kovac T, Kovac M, Has-Schön E. Biological study on novel coumarinyl 1, 3, 4-oxadiazoles. Turkish journal of chemistry. 2018;42(1):146–57.
25. Mustafa YF. Coumarins from toxic phenol: An algorithm of their synthesis and assessment as biosafe, wide-spectrum, potent antimicrobial prospects. Applied Chemical Engineering. 2024;7(3):5527.
26. Ostrowska K. Coumarin-piperazine derivatives as biologically active compounds. Saudi Pharmaceutical Journal. 2020;28(2):220–32.
27. Waheed SA, Mustafa YF. Benzocoumarin backbone is a multifunctional and affordable scaffold with a vast scope of biological activities. Journal of Medicinal and Chemical Sciences. 2022;5(5):703–21.
28. Mustafa YF, Faisal AF, Alshaher MM, Hassan DA. Food-Derived Micronutrients as Alleviators of Age-Related Dysfunction: A Dive into Their Effects and Cellular Mechanisms. Indian Journal of Clinical Biochemistry. 2025; https://doi.org/10.1007/s12291-024-01297-7
29. Sashidhara K V., Modukuri RK, Singh S, Bhaskara Rao K, Aruna Teja G, Gupta S, Shukla S. Design and synthesis of new series of coumarin-aminopyran derivatives possessing potential anti-depressant-like activity. Bioorganic and Medicinal Chemistry Letters. 2015;25(2):337–41.
30. Zeki NM, Mustafa YF. 6,7-Coumarin-heterocyclic hybrids: A comprehensive review of their natural sources, synthetic approaches, and bioactivity. Journal of Molecular Structure. 2024;1303:137601.
31. Mustafa YF, Al-Shakarchi W. The psychotropic potential of coumarins: Mechanisms, efficacy, and future prospects. Environment and Social Psychology. 2025;10(3):3534.
32. Kartsev V, Geronikaki A, Bua S, Nocentini A, Petrou A, Lichitsky B, Frasinyuk M, Leitans J, Kazaks A, Tars K, Supuran CT. Extending the Inhibition Profiles of Coumarin-Based Compounds Against Human Carbonic Anhydrases: Synthesis, Biological, and In Silico Evaluation. Molecules. 2019;24(19):3580.
33. Khalil RR, Mohammed ET, Mustafa YF. Various promising biological effects of Cranberry extract: A review. Clinical Schizophrenia and Related Psychoses. 2021;15(S6):1–9.
34. Jibroo RN, Mustafa YF, Al-Shakarchi W. Heterocycles fused on a 6,7-coumarin framework: an in-depth review of their structural and pharmacological diversity. Chemical Papers. 2024;78:7239–7311.
35. Jebir RM, Mustafa YF. Natural products catalog of allsweet watermelon seeds and evaluation of their novel coumarins as antimicrobial candidates. Journal of Medicinal and Chemical Sciences. 2022;5(5):831–47.
36. Ismael RN, Mustafa YF, Al-Qazaz HK. Citrullus lanatus, a Potential Source of Medicinal Products: A Review. Journal of Medicinal and Chemical Sciences. 2022;5(4):607–18.
37. Mustafa YF, Bashir MK, Oglah MK. Influence of albocarbon-cyclic hybridization on biomedical activities: A review. Journal of Medicinal and Chemical Sciences. 2022;5(4):518–35.
38. Jasim SF, Mustafa YF. A Review of Classical and Advanced Methodologies for Benzocoumarin Synthesis. Journal of Medicinal and Chemical Sciences. 2022;5(5):676–94.
39. Mustafa YF, Khalil RR, Mohammed ET. Synthesis and antitumor potential of new 7-halocoumarin-4-acetic acid derivatives. Egyptian Journal of Chemistry. 2021;64(7):3711–6.
40. Mustafa YF. Synthesis of 7,8-dihydroxy-4-phenylbenzo[g]coumarins as potential multitarget anti-skin-aging candidates. Journal of Molecular Structure. 2025;1321:139806.
41. Younes AH, Mustafa YF. Plant-Derived Coumarins: A Narrative Review Of Their Structural And Biomedical Diversity. Chemistry & Biodiversity. 2024;21(6):e202400344.
42. Abdulaziz NT, Mohammed ET, Khalil RR, Mustafa YF. Unrevealing the total phenols, total flavonoids, antioxidant, anti-inflammatory, and cytotoxic effects of Garden Cress seed ethanolic extracts. Review of Clinical Pharmacology and Pharmacokinetics - International Edition. 2024;38(2):187–96.
43. Ban AA, Ibrahim BY, Mustafa YF. The Protective Role of Natural Coumarins Derivatives and Anpro Supplement Against Aflatoxin B1 Pollution in the Quails Coturnix Japonica Diet. Mesopotamia Journal of Agriculture. 2023;51(1):1–13.
44. Gangopadhyay A. Plant-derived natural coumarins with anticancer potentials: future and challenges. Journal of Herbal Medicine. 2023;42:100797.
45. Zeki NM, Mustafa YF. Synthesis and Pharmacological Profiles of 6,7-Dihydroxycoumarin and Its Derivatives: A Concise Review. Iraqi Journal of Pharmacy. 2023;20(Supplementary Issue 1):174–88.
46. Hussain MK, Khatoon S, Khan MF, Akhtar MS, Ahamad S, Saquib M. Coumarins as versatile therapeutic phytomolecules: A systematic review. Phytomedicine. 2024;134:155972.
47. Faisal AF, Fakri Mustafa Y. The role of coumarin scaffold in the chemical engineering of bioactive molecules: A narrative review. Applied Chemical Engineering. 2025;8(1):5595.

48. Buckner CA, Lafrenie RM, Dénommée JA, Caswell JM, Want DA. Complementary and alternative medicine use in patients before and after a cancer diagnosis. Current Oncology. 2018;25(4):e275–81.
49. Alshaher MM, Mustafa YF. Synthesis of triclosan-derived coumarins as potent, biocompatible, broad-spectrum antimicrobial agents. Applied Chemical Engineering. 2024;7(4):5579.
50. Ma QJ, Zhang XB, Zhao XH, Jin Z, Mao GJ, Shen GL, Yu RQ. A highly selective fluorescent probe for Hg2+ based on a rhodamine–coumarin conjugate. Analytica Chimica Acta. 2010;663(1):85–90.
51. Satpati AK, Kumbhakar M, Nath S, Pal H. Photophysical Properties of Coumarin-7 Dye: Role of Twisted Intramolecular Charge Transfer State in High Polarity Protic Solvents. Photochemistry and Photobiology. 2009;85(1):119–29.
52. Cohen SM, Ellwein LB. Genetic Errors, Cell Proliferation, and Carcinogenesis. Cancer Research. 1991;51(24):6493–505.
53. Mustafa YF. Role of Fruit-Derived Antioxidants in Fighting Cancer: A Narrative Review. Indian Journal of Clinical Biochemistry. 2025;e70321. https://doi.org/10.1007/s12291-025-01310-7
54. Alshaher MM, Mustafa YF. Linear pyranocoumarins are potential dazzling dancers between nature, chemistry, and clinical application. Phytomedicine Plus. 2025;5(2):100785.
55. Jibroo RN, Mustafa YF. Linearly ring-fused coumarins: A review of their cancer-fighting attributes. Results in Chemistry. 2024;8:101611.
56. Mustafa YF, Ismael RN, Jebir RM. Natural coumarins from two cultivars of watermelon seeds as biosafe anticancer agents, an algorithm for their isolation and evaluation. Journal of Molecular Structure. 2024;1295(P1):136644.
57. Zeki NM, Mustafa YF. Coumarin hybrids for targeted therapies: A promising approach for potential drug candidates. Phytochemistry Letters. 2024;60:117–33.
58. Jebir MR, Mustafa YF. Kidney stones: natural remedies and lifestyle modifications to alleviate their burden. International Urology and Nephrology. 2024;56(3):1025–33.
59. Hayes DG, Williams M, Pechacek N, Hebert B, Stanton K. Precise measurement of 1,4-dioxane concentration in cleaning products: A review of the current state-of-the-art. Vol. 25, Journal of Surfactants and Detergents. 2022. p. 729–41.
60. Chen R, Liu C, Johnson NW, Zhang L, Mahendra S, Liu Y, Dong Y, Chen M. Removal of 1,4-dioxane by titanium silicalite-1: Separation mechanisms and bioregeneration of sorption sites. Chemical Engineering Journal. 2019;371:193–202.
61. Palumbo B, Conrad-Vlasak D, Stanton K. A novel protocol for quantitative determination of 1,4-dioxane in finished cleaning products. Journal of Surfactants and Detergents. 2023;26(4):565–76.
62. Aped P, Apeloig Y, Ellencweig A, Fuchs B, Goldberg I, Karni M, Tartakovsky E. Structure and conformation of heterocycles. 16. Probing the anomeric effect. Trimethylsilyloxy and tert-butoxy substituents in 1, 4-dioxane derivatives: theory vs. experiment. Journal of the American Chemical Society. 1987;109(5):1486–95.
63. Patra I, Ansari MJ, Saadoon N, Mashhadani ZI Al, Obaid NH, Alawsi T, Jabbar AH, Mustafa YF. Insights into the Electronic Properties of Coumarins: A Comparative Study Photocatalytic Degradation of Methylene Blue. Physical Chemistry Research. 2023;11(2):437–47.
64. Ahmed B, Khan SA, Alam T. Synthesis and antihepatotoxic activity of some heterocyclic compounds containing the 1, 4-dioxane ring system. Die Pharmazie-An International Journal of Pharmaceutical Sciences. 2003;58(3):173–6.
65. Godri Pollitt KJ, Kim JH, Peccia J, Elimelech M, Zhang Y, Charkoftaki G, Hodges B, Zucker I, Huang H, Deziel NC, Murphy K, Ishii M, Johnson CH, Boissevain A, O'Keefe E, Anastas PT, Orlicky D, Thompson DC, et al. 1,4-Dioxane as an emerging water contaminant: State of the science and evaluation of research needs. Science of The Total Environment. 2019;690:853–66.
66. Mustafa YF. 3-mercaptocoumarins as potential bioactive candidates: From novel synthesis to comparative analysis. Journal of Molecular Structure. 2025;1320:139657.
67. Mustafa YF. Synthesis of novel 6-aminocoumarin derivatives as potential –biocompatible antimicrobial and anticancer agents. Journal of Molecular Structure. 2025;1320:139658.
68. Ahmed BA, Mustafa YF, Ibrahim BY. Isolation and characterization of furanocoumarins from Golden Delicious apple seeds. Journal of Medicinal and Chemical Sciences. 2022;5(4):537–45.
69. Ismael SS, Waheed NAM, Kasim SM, Mustafa YF. Novel Coumarin-Indole Hybrids as Cytotoxic Candidates: Synthesis and Antiproliferative Activity. Pharmacognosy Journal. 2023;15(6):1105–11.
70. Potapov AY, Paponov B V., Podoplelova NA, Panteleev MA, Potapov MA, Ledenyova I V., Stolpovskaya N V., Shikhaliev KS. Synthesis of 2H-pyrano[3,2-g]quinolin-2-ones containing a pyrimidinone moiety and characterization of their anticoagulant activity via inhibition of blood coagulation factors Xa and XIa. Chemistry of Heterocyclic Compounds. 2021;57(5):574–80.
71. Mustafa YF, Zain Al-Abdeen SH, Khalil RR, Mohammed ET. Novel functionalized phenyl acetate derivatives of benzo [e]-bispyrone fused hybrids: Synthesis and biological activities. Results in Chemistry. 2023;5:100942.
72. Patra P. A short review on the synthesis of pyrrolo[3,4- c]coumarins an isolamellarin-B scaffolds. Synthetic Communications. 2022;52(21):1999–2018.

73. Jamalis J, Yusof FSM, Chander S, Wahab RA, P. Bhagwat D, Sankaranarayanan M, Almalki F, Hadda T Ben. Psoralen Derivatives: Recent Advances of Synthetic Strategy and Pharmacological Properties. Anti-Inflammatory & Anti-Allergy Agents in Medicinal Chemistry. 2020;19(3):222–39.
74. Jiang C, Guo J, Wang Z, Xiao B, Lee HJ, Lee EO, Kim SH, Lu J. Decursin and decursinol angelate inhibit estrogen-stimulated and estrogen-independent growth and survival of breast cancer cells. Breast Cancer Research. 2007;9(6):1–12.
75. Prateeptongkum S, Mahavorasirikul W, Duangdee N. Synthesis and anti-proliferative activity of novel oxepin-annulated coumarins. Arkivoc. 2018;2018(7):73–85.
76. Vlachou EN, Armatas GS, Litinas KE. Synthesis of Fused Oxazolocoumarins from o -Hydroxynitrocoumarins and Benzyl Alcohol Under Gold Nanoparticles or FeCl 3 Catalysis. Journal of Heterocyclic Chemistry. 2017;54(4):2447–53.
77. Jasim SF, Mustafa YF. Synthesis and Antidiabetic Assessment of New Coumarin-Disubstituted Benzene Conjugates: An In Silico-In Virto Study. Journal of Medicinal and Chemical Sciences. 2022;5(6):887–99.
78. Jasim SF, Mustafa YF. New fused-coumarin composites: Synthesis, anticancer and antioxidant potentials evaluation. Eurasian Chemical Communications. 2022;4(7):607–19.
79. Jasim SF, Mustafa YF. Synthesis, ADME Study, and antimicrobial evaluation of novel naphthalene-based derivatives. Journal of Medicinal and Chemical Sciences. 2022;5(5):793–807.
80. Waheed SA, Mustafa YF. The in vitro effects of new albocarbon-based coumarins on blood glucose-controlling enzymes. Journal of Medicinal and Chemical Sciences. 2022;5(6):954–67.
81. Waheed SA, Mustafaa YF. Novel naphthalene-derived coumarin composites: synthesis, antibacterial, and antifungal activity assessments. Eurasian Chemical Communications. 2022;4(8):709–24.
82. Waheed SA, Mustafa YF. Synthesis and evaluation of new coumarins as antitumor and antioxidant applicants. Journal of Medicinal and Chemical Sciences. 2022;5(5):808–19.
83. Jibroo RN, Mustafa YF, Al-Shakarchi W. Synthesis and evaluation of linearly fused thiadiazolocoumarins as prospects with broad-spectrum bioactivity. Results in Chemistry. 2024;7:101494.
84. Zeki NM, Mustafa YF. Novel heterocyclic coumarin annulates: synthesis and figuring their roles in biomedicine, bench-to-bedside investigation. Chemical Papers. 2024;78:4935–51.
85. Zeki NM, Mustafa YF. Synthesis of Novel Dioxathiole-6,7-coumarin Hybrids As Cytosafe-Multifunctional Applicants: An In Vitro—In Silico Study. Russian Journal of Bioorganic Chemistry. 2024;50(5):2076–91.
86. Zeki MN, Mustafa YF. Synthesis and evaluation of novel ring-conjugated coumarins as biosafe broad-spectrum antimicrobial candidates. Journal of Molecular Structure. 2024;1309:138192.
87. Zeki NM, Mustafa YF. Coumarin hybrids: a sighting of their roles in drug targeting. Chemical Papers. 2024;78:5753–5772.
88. Mazin Zeki N, Fakri Mustafa Y. Annulated Heterocyclic[g]Coumarin Composites: Synthetic Approaches and Bioactive Profiling. Chemistry & Biodiversity. 2024;21(3):e202301855.
89. Chapleo CB, Doxey JC, Myers PL, Myers M, Smith CFC, Stillings MR. Effect of 1, 4 Dioxanyl Substitution on the Adrenergic Activity of Some Standard Adrenoreceptor Agents. European Journal of Medicinal Chemistry. 1989;24(6):619.
90. Mustafa YF. Synthesis, in silico analysis, and biomedical effects of coumarins derived from resveratrol. Phytomedicine Plus. 2024;3(4):100501.
91. Mustafa YF, Hassan DA, Faisal AF, Alshaher MM. Synthesis of novel skipped diene-3-halocoumarin conjugates as potent anticancer and antibacterial biocompatible agents. Results in Chemistry. 2024;11:101846.
92. Mustafa YF. Triple coumarin-based 5-fluorouracil prodrugs, their synthesis, characterization, and release kinetics. Journal of Molecular Structure. 2024;1301:137415.
93. Kamal IK, Mahmood AT, Mustafa YF. Synthesis of Eugenol-Derived Coumarins as Broad-Spectrum Biosafe Antimicrobial Agents. Russian Journal of Bioorganic Chemistry. 2024;50(6):2240–51.
94. Ransy C, Vaz C, Lombès A, Bouillaud F. Use of H2O2 to cause oxidative stress, the catalase issue. International Journal of Molecular Sciences. 2020;21(23):9149.
95. Mustafa YF. Biocompatible chlorocoumarins from harmful chlorophenols, their synthesis and biomedicinal evaluation. Journal of Molecular Structure. 2024;1309:138193.
96. Khalil RR, Mohammed ET, Mustafa YF. Evaluation of in vitro antioxidant and antidiabetic properties of Cydonia Oblonga seeds' extracts. Journal of Medicinal and Chemical Sciences. 2022;5(6):1048–58.
97. Abdelbasset WK, Elkholi SM, Ismail KA, AL-Ghamdi HS, Mironov S, Ridha HSH, Maashi MS, Thangavelu L, Mahmudiono T, Mustafa YF. Mequinol-loaded carboxymethyl cellulose/chitosan electrospun wound dressing as a potential candidate to treat diabetic wounds. Cellulose. 2022;29(14):7863–81.
98. Huldani H, Kozlitina IA, Alshahrani M, Daabo HMA, Almalki SG, Oudaha KH, Alawadi AH, Alsalamy A, Joshi SK, Mustafa YF. Exosomes derived from adipose stem cells in combination with hyaluronic acid promote diabetic wound healing. Tissue and Cell. 2023;85:102252.
99. Abdelbasset WK, Jasim SA, Sharma SK, Margiana R, Bokov DO, Obaid MA, Hussein BA, Lafta HA, Jasim SF, Mustafa YF. Alginate-Based Hydrogels and Tubes, as Biological Macromolecule-Based Platforms for Peripheral Nerve Tissue Engineering: A Review. Annals of Biomedical Engineering. 2022;50(6):628–53.

100. Roomi AB, Widjaja G, Savitri D, Jalil AT, Mustafa YF, Thangavelu L, Kazhibayeva G, Suksatan W, Chupradit S, Aravindhan S. SnO2:Au/Carbon Quantum Dots Nanocomposites: Synthesis, Characterization, and Antibacterial Activity. Journal of Nanostructures. 2021;11(3):514–23.
101. Mustafa YF. Emerging trends and future opportunities for coumarin-heterocycle conjugates as antibacterial agents. Results in Chemistry. 2023;6:101151.
102. Mahmood AT, Kamal IK, Mustafa YF. Coumarin Backbone as a Door-Opening Key for Investigating Chloroxylenol as Oral Antimicrobial Agents: an In Vitro–In Silico Study. Russian Journal of Bioorganic Chemistry. 2024;50(6):2252–68.
103. Al Abdeen SHZ, Mustafa YF, Mutlag SH. Synthesis and biomedical activities of novel multifunctional benzodipyrone-based derivatives. Eurasian Chemical Communications. 2022;4(10):938–49.
104. Kasim SM, Abdulaziz NT, Mustafa YF. Synthesis and biomedical activities of coumarins derived from natural phenolic acids. Journal of Medicinal and Chemical Sciences. 2022;5(4):546–60.
105. Abdulaziz NT, Mustafa YF. Antibacterial and Antitumor Potentials of Some Novel Coumarins. International Journal of Drug Delivery Technology. 2022;12(1):239–47.
106. Ismael RN, Mustafa YF, Al-Qazaz HK. Cancer-curative potential of novel coumarins from watermelon princess: A scenario of their isolation and activity. Eurasian Chemical Communications. 2022;4(7):657–72.
107. Amin KM, Eissa AAM, Abou-Seri SM, Awadallah FM, Hassan GS. Synthesis and biological evaluation of novel coumarin-pyrazoline hybrids endowed with phenylsulfonyl moiety as antitumor agents. European Journal of Medicinal Chemistry. 2013;60:187–98.
108. Mustafa YF. 4-Chloroskimmetine-based derivatives as potential anticancer and antibacterial prospects: Their synthesis and in vitro inspections. Results in Chemistry. 2024;7:101511.
109. Mustafa YF. Modern Developments in the Application and Function of Metal/Metal Oxide Nanocomposite–Based Antibacterial Agents. BioNanoScience. 2023;13:840–52.
110. Mustafa YF. Synthesis, characterization, and biomedical assessment of novel bisimidazole–coumarin conjugates. Applied Nanoscience (Switzerland). 2023;13(3):1907–18.
111. Mustafa YF, Najem MA, Tawffiq ZS. Coumarins from Creston apple seeds: Isolation, chemical modification, and cytotoxicity study. Journal of Applied Pharmaceutical Science. 2018;8(8):49–56.
112. Jasim MHM, Mustafa YF. Synthesis of Acetaminophen-Based Coumarins as Selective COX-2 Inhibitors: An in vitro-in silico Study. Chemistry & Biodiversity. 2024;21(10):e202401309.
113. Mustafa YF. Synthesis, characterization and preliminary cytotoxic study of sinapic acid and its analogues. Journal of Global Pharma Technology. 2019;11(9):1–10.
114. Mahmood AAJ, Mustafa YF, Abdulstaar M. New coumarinic azo-derivatives of metoclopramide and diphenhydramine: Synthesis and in vitro testing for cholinesterase inhibitory effect and protection ability against chlorpyrifos. International Medical Journal Malaysia. 2014;13(1):3–12.
115. Hunagund UB. A Study on Synthesis and Biological Activities of Novel Heterocyclic Compounds. International Journal of Research Publication and Reviews. 2024;5(7):1151–9.
116. Nicolaou KC. Advancing the Drug Discovery and Development Process. Angewandte Chemie. 2014;126(35):9280–92.
117. Marfavi A, Kavianpour P, Rendina LM. Carboranes in drug discovery, chemical biology and molecular imaging. Nature Reviews Chemistry. 2022;6(7):486–504.
118. Li X, Shen X, Jiang W, Xi Y, Li S. Comprehensive review of emerging contaminants: Detection technologies, environmental impact, and management strategies. Ecotoxicology and Environmental Safety. 2024;278:116420.
119. Younes HA, Mustafa YF. Sweet Bell Pepper: A Focus on Its Nutritional Qualities and Illness-Alleviated Properties. Indian Journal of Clinical Biochemistry. 2024;39:459–69.
120. Lam TP, Tran NVN, Pham LHD, Lai NVT, Dang BTN, Truong NLN, Nguyen-Vo SK, Hoang TL, Mai TT, Tran TD. Flavonoids as dual-target inhibitors against α-glucosidase and α-amylase: a systematic review of in vitro studies. Natural Products and Bioprospecting. 2024;14(1):4.
121. Jebir RM, Mustafa YF. Novel coumarins isolated from the seeds of Citrullus lanatus as potential antimicrobial agents. Eurasian Chemical Communications. 2022;4(8):692–708.
122. Basanagouda M, Jambagi VB, Barigidad NN, Laxmeshwar SS, Devaru V, Narayanachar. Synthesis, structure–activity relationship of iodinated-4-aryloxymethyl-coumarins as potential anti-cancer and anti-mycobacterial agents. European Journal of Medicinal Chemistry. 2014;74:225–33.
123. Sunthitikawinsakul A, Kongkathip N, Kongkathip B, Phonnakhu S, Daly JW, Spande TF, Nimit Y, Rochanaruangrai S. Coumarins and Carbazoles from Clausena excavata Exhibited Antimycobacterial and Antifungal Activities. Planta Medica. 2003;69(2):155–7.
124. Morrison R, Al-Rawi JMA. Synthesis, structure elucidation, DNA-PK, PI3K, anti-platelet and anti-bacteria activity of linear 5, 6, and 10-substituted-2-morpholino-chromen-oxazine-dione and angular 3, 4, 6-substituted-8-morpholino-chromen-oxazine-2,10-dione. Journal of Enzyme Inhibition and Medicinal Chemistry. 2016;31:86–95.
125. Yadav P, Kumar B, Gautam HK, Sharma SK. Synthesis and antibacterial activity screening of quaternary ammonium derivatives of triazolyl pyranochromenones. Journal of Chemical Sciences. 2017;129(2):211–22.

126. Lipeeva A V., Zakharov DO, Burova LG, Frolova TS, Baev DS, Shirokikh I V., Evstropov AN, Sinitsyna OI, Tolsikova TG, Shults EE. Design, Synthesis and Antibacterial Activity of Coumarin-1,2,3-triazole Hybrids Obtained from Natural Furocoumarin Peucedanin. Molecules. 2019;24(11):21–6.
127. Mustafa YF, Waheed SA, Jasim SF, Jebir RM, Ismael RN, Qutachi O. A Narrative Review of Benzo-Fused Coumarins, Shedding Light on Their Medicinal Activities. Iraqi Journal of Pharmacy. 2023;20(1):7–16.
128. Molchanova N, Nielsen JE, Sørensen KB, Prabhala BK, Hansen PR, Lund R, Barron AE, Jenssen H. Halogenation as a tool to tune antimicrobial activity of peptoids. Scientific Reports. 2020;10(1):1–10.
129. Shinada NK, de Brevern AG, Schmidtke P. Halogens in protein–ligand binding mechanism: A structural perspective. Journal of Medicinal Chemistry. 2019;62(21):9341–56.
130. Kosikowska U, Wujec M, Trotsko N, Płonka W, Paneth P, Paneth A. Antibacterial activity of fluorobenzoylthiosemicarbazides and their cyclic analogues with 1,2,4-triazole scaffold. Molecules (Basel, Switzerland). 2020;26(1):1–18.
131. Zi Y, Zhu M, Li X, Xu Y, Wei H, Li D, Mu C. Effects of carboxyl and aldehyde groups on the antibacterial activity of oxidized amylose. Carbohydrate Polymers. 2018;192:118–25.
132. Kasim SM, Abdulaziz NT, Jasim MH, Mustafa YF. Resveratrol in cancer chemotherapy: Is it a preventer, protector, or fighter? Eurasian Chemical Communications. 2023;5(7):576–87.
133. Zhu Y, Yao X, Long J, Li R, Liu Y, Yang Z, Zheng X. Fluorine-Containing Chrysin Derivatives. Natural Product Communications. 2019;14(9):1–11.
134. Auti PS, George G, Paul AT. Recent advances in the pharmacological diversification of quinazoline/quinazolinone hybrids. RSC Advances. 2020;10(68):41353–92.
135. Al-Harthy T, Zoghaib W, Abdel-Jalil R. Importance of Fluorine in Benzazole Compounds. Molecules. 2020;25(20):4677.
136. Freire RLM, Marques MB de F, Souza-Fagundes EM de, Oliveira RB de, Alves RJ. Synthesis and evaluation of platinum complexes with potential antitumor activity. Brazilian Journal of Pharmaceutical Sciences. 2017;53(1):e15235.
137. Valicherla GR, Dave KM, Syed AA, Riyazuddin M, Gupta AP, Singh A, Wahajuddin MK, Datta D, Gayen JR. Formulation optimization of docetaxel loaded self-emulsifying drug delivery system to enhance bioavailability and anti-tumor activity. Scientific Reports. 2016; 6: 26895.
138. Shi J, Li J, Xu Z, Chen L, Luo R, Zhang C, Gao F, Zhang J, Fu C. Celastrol: A Review of Useful Strategies Overcoming its Limitation in Anticancer Application. Frontiers in Pharmacology. 2020;11:558741.
139. Meier-Menches SM, Gerner C, Berger W, Hartinger CG, Keppler BK. Structure–activity relationships for ruthenium and osmium anticancer agents – towards clinical development. Chemical Society Reviews. 2018;47(3):909–28.
140. Mirghani R, Saba T, Khaliq H, Mitchell J, Do L, Chambi L, Diaz K, Kennedy T, Alkassab K, Huynh T, Elmi M, Martinez J, Sawan S, Rijal G. Biofilms: Formation, drug resistance and alternatives to conventional approaches. AIMS Microbiology. 2022;8(3):239–77.
141. Al-Shakarchi W, Saber Y, Merkhan MM, Mustafa YF. Sub Chronic Toxicity Study of Coumacines. Pharmacognosy Journal. 2023;15(1):160–4.
142. Naik NS, Shastri LA, Joshi SD, Dixit SR, Chougala BM, Samundeeswari S, Holiyachi M, Shaikh F, Madar J, Kulkarni R, Sunagar V. 3,4-Dihydropyrimidinone-coumarin analogues as a new class of selective agent against S. aureus: Synthesis, biological evaluation and molecular modelling study. Bioorganic and Medicinal Chemistry. 2017;25(4):1413–22.
143. Rim KT. In silico prediction of toxicity and its applications for chemicals at work. Toxicology and Environmental Health Sciences. 2020;12(3):191–202.
144. Rioux B, Mention MM, Alarcan J, Abiola TT, Peyrot C, Brunissen F, Braeuning A, Stavros VG, Allais F. Sustainable synthesis, in silico evaluation of potential toxicity and environmental fate, antioxidant and UV-filtering/photostability activity of phenolic-based thiobarbituric derivatives. Green Chemistry Letters and Reviews. 2022;15(1):116–27.
145. Setia Budi H, Javed Ansari M, Abdalkareem Jasim S, Abdelbasset WK, Bokov D, Fakri Mustafa Y, Najm MAA, Kazemnejadi M. Preparation of antibacterial Gel/PCL nanofibers reinforced by dicalcium phosphate-modified graphene oxide with control release of clindamycin for possible application in bone tissue engineering. Inorganic Chemistry Communications. 2022;139:109336.
146. Zeki NM, Mustafa YF. Digital alchemy: Exploring the pharmacokinetic and toxicity profiles of selected coumarin-heterocycle hybrids. Results in Chemistry. 2024;10:101754.
147. van de Waterbeemd H, Gifford E. ADMET in silico modelling: Towards prediction paradise? Nature Reviews Drug Discovery. 2003;2(3):192–204.
148. Muehlbacher M, Spitzer GM, Liedl KR, Kornhuber J. Qualitative prediction of blood–brain barrier permeability on a large and refined dataset. Journal of Computer-Aided Molecular Design. 2011;25(12):1095–106.
149. Mustafa YF, Abdulaziz NT. Anticancer potential of hymecromone-based compounds: A review. Biochemical and Cellular Archives. 2021;21(2):4151–61.
150. Hernandez-Gordillo V, Koppes AN, Griffith LG, Breault DT, Carrier RL. Engineering the Niche for Intestinal Regeneration. Biology and Engineering of Stem Cell Niches. 2017;601–15.

151. Artursson P, Palm K, Luthman K. Caco-2 monolayers in experimental and theoretical predictions of drug transport1PII of original article: S0169-409X(96)00415-2. The article was originally published in Advanced Drug Delivery Reviews 22 (1996) 67–84.1. Advanced Drug Delivery Reviews. 2001;46(1–3):27–43.
152. Zhou SF. Drugs behave as substrates, inhibitors and inducers of human cytochrome P450 3A4. Current Drug Metabolism. 2008;9(4):310–22.
153. Mustafa YF, Bashir MK, Oglah MK. Synthesis, antioxidant and antitumor activities of new coumarins grafted to 5-fluorouracil. Caspian Journal of Environmental Sciences. 2022;20(2):359–65.
154. Van Booven D, Marsh S, McLeod H, Carrillo MW, Sangkuhl K, Klein TE, Altman RB. Cytochrome P450 2C9-CYP2C9. Pharmacogenetics and Genomics. 2010;20(4):277–81.
155. Al-Shakarchi W, Saber Y, Merkhan M, Mustafa Y. Acute toxicity of coumacines: An in vivo study. Georgian medical news. 2023;(338):126–31.
156. Hariyanti T, Margiana R, Al-Gazally ME, Patra I, Lateef Al-Awsi GR, Hameed N, Kayumova D, Ansari MJ, Torres-Criollo LM, Mustafa YF, Abedi-Firouzjah R, Farhood B. The Protective Effects of Silymarin on the Reproductive Toxicity: A Comprehensive Review. Current Medicinal Chemistry. 2023;30(39):4421–49.
157. Zhou S, Zhao FL, Wang SH, Wang YR, Hong Y, Zhou Q, Geng PW, Luo QF, Cai JP, Dai DP. Assessments of CYP-inhibition-based drug–drug interaction between vonoprazan and poziotinib in vitro and in vivo. Pharmaceutical Biology. 2023;61(1):356–61.
158. Zhou ZW, Zhou SF. Application of mechanism-based CYP inhibition for predicting drug–drug interactions. Expert Opinion on Drug Metabolism & Toxicology. 2009;5(6):579–605.
159. Huldani H, Rashid AI, Turaev KN, Opulencia MJC, Abdelbasset WK, Bokov DO, Mustafa YF, Al-Gazally ME, Hammid AT, Kadhim MM, Ahmadi SH. Concanavalin A as a promising lectin-based anti-cancer agent: the molecular mechanisms and therapeutic potential. Cell Communication and Signaling. 2022;20(1):1–14.
160. Rohmah MK, Salahdin OD, Gupta R, Muzammil K, Qasim MT, Al-qaim ZH, Abbas NF, Jawad MA, Yasin G, Mustafa YF, Heidary A, Abarghouei S. Modulatory role of dietary curcumin and resveratrol on growth performance, serum immunity responses, mucus enzymes activity, antioxidant capacity and serum and mucus biochemicals in the common carp, Cyprinus carpio exposed to abamectin. Fish and Shellfish Immunology. 2022;129:221–30.
161. Zamanian MY, Parra RMR, Soltani A, Kujawska M, Mustafa YF, Raheem G, Al-Awsi L, Lafta HA, Taheri N, Heidari M, Golmohammadi M, Bazmandegan G. Targeting Nrf2 signaling pathway and oxidative stress by resveratrol for Parkinson's disease: an overview and update on new developments. Molecular Biology Reports. 2023;50:5455–5464.
162. Benet LZ, Hosey CM, Ursu O, Oprea TI. BDDCS, the Rule of 5 and drugability. Advanced Drug Delivery Reviews. 2016;101:89–98.
163. Hachem K, Jasim SA, Al-Gazally ME, Riadi Y, Yasin G, Turki Jalil A, Abdulkadhm MM, Saleh MM, Fenjan MN, Mustafa YF, Dehno Khalaji A. Adsorption of Pb(II) and Cd(II) by magnetic chitosan-salicylaldehyde Schiff base: Synthesis, characterization, thermal study and antibacterial activity. Journal of the Chinese Chemical Society. 2022;69(3):512–21.
164. Andrew F, Peter P. P-glycoprotein and its role in drug-drug interactions. Ustralian Prescriber. 2014;37(4):137–9.
165. Mustafa YF, Alshaher, Marwa Mohammed Hassan DA, Faisal AF. Synthesis and Medicinal Impacts of Novel 3,3′-Bihalocoumarins and Their Precursors , 7-Halocoumarin-3-acetic Acids. Russian Journal of Bioorganic Chemistry. 2025;51(2):802–15.
166. Ghafourian T, Amin Z. QSAR models for the prediction of plasma protein binding. BioImpacts. 2013;3(1):21–7.
167. Mazin Zeki N, M. Z. Othman K, Fakri Mustafa Y. Computational Chemistry: A game-changer in the drug discovery field. Applied Chemical Engineering. 2025;8(1):5601.
168. Mohammed Alshaher M, Fakri Mustafa Y. From laboratory to computer models: Enhancing coumarin discovery through interdisciplinary research. Applied Chemical Engineering. 2025;8(1):5613.
169. Singh A, Worku ZA, Van den Mooter G. Oral formulation strategies to improve solubility of poorly water-soluble drugs. Expert Opinion on Drug Delivery. 2011;8(10):1361–78.
170. Aungst BJ. Optimizing Oral Bioavailability in Drug Discovery: An Overview of Design and Testing Strategies and Formulation Options. Journal of Pharmaceutical Sciences. 2017;106(4):921–9.
171. Fakri Mustafa Y, Hassan DA. Dioxolocoumarins: Bridging chemistry and pharmacology with multifunctional therapeutics. Applied Chemical Engineering. 2024;7(4):5592.
172. Abadie A. Using synthetic controls: Feasibility, data requirements, and methodological aspects. Journal of economic literature. 2021;59(2):391–425.
173. Kasim SM, Al-Dabbagh BM, Mustafa YF. A review on the biological potentials of carbazole and its derived products. Eurasian Chemical Communications. 2022;4(6):495–512.
174. Abdulaziz NT, Al-bazzaz FY, Mustafa YF. Natural products for attenuating Alzheimer's disease: A narrative review. Eurasian Chemical Communications. 2023;5(4):358–70.
175. Al-Shakarchi W, Abdulaziz NT, Mustafa YF. A review of the chemical, pharmacokinetic, and pharmacological aspects of quercetin. Eurasian Chemical Communications. 2022;4(7):645–56.